THE PENNSYLVANIA STATE UNIVERSITY
SCHREYER HONORS COLLEGE

DEPARTMENT OF MECHANICAL AND NUCLEAR ENGINEERING

NUMERICAL MODELLING OF A ROTARY VANE EXPANDER FOR A POWER CYCLE ON A PROPOSED LANDED MISSION TO VENUS

TAMUNO-NEGIYEOFORI BRYANT WARMATE
SPRING 2018

A thesis
submitted in partial fulfillment
of the requirements
for a baccalaureate degree
in Mechanical Engineering
with honors in Mechanical Engineering

Reviewed and approved* by the following:

Alex Rattner
Assistant Professor, Mechanical and Nuclear Engineering
Thesis Supervisor

Daniel Cortes
Assistant Professor, Mechanical and Nuclear Engineering
Honors Adviser

* Signatures are on file in the Schreyer Honors College.

ABSTRACT

Exploring Venus is a daunting task due to its extreme ambient conditions: a surface temperature exceeding 800K, high atmospheric pressure (about 90 bar), and high levels of atmospheric sulfur. This environment necessitates unconventional power generation approaches. Conventional power generating turbomachinery such as radial flow turbines, are expensive, require extreme rotation rates at planetary lander capacities, and are sensitive to two-phase flow (condensation). Rotary vane expanders can operate in mixed flow, operate at low rotational speed, and minimizes mechanical complexity, thereby reducing the likelihood of failure. The operating characteristics of a rotary vane expander are suitable for a small-scale system that can be incorporated into a lander-scale Rankine power system (100 W to 10kW). Additionally, traditional Rankine cycle working fluids (*e.g.*, water/steam) would not be feasible as they would be supercritical at ambient conditions. The robustness of rotary vane expanders allows for the use of exotic working fluids such as vapor mercury. However, limited research has been done to explore the operational capabilities of using exotic working fluid in a rotary vane expander. Therefore, developing a computational model to estimate the performances and capabilities is the first critical step to determining the feasibility of the system. Two dynamic and adaptable models were developed to analyze the performance of rotary vane expanders in this application. The first model characterizes the expander at the individual working chamber and vane scale at a given operating condition. The second higher level model maps the power, torque, and efficiency over various operating conditions. The performance plots were comparable to those of similarly sized rotary vane expanders, but further validation is required.

TABLE OF CONTENTS

LIST OF FIGURES

LIST OF TABLES

ACKNOWLEDGEMENTS

I would first like to thank Dr. Alexander Rattner (honors supervisor), Chris Geer (Ph.D. candidate) and entire Multiscale Thermal Fluids and Energy (MTFE) research group for the opportunity to be part of this project. Their dedication and genuine interest in making an impact spurred me on through all the difficulties. Additionally, I would like to thank, Dr. Daniel Cortes, the Schreyer advisors and the entire Mechanical and Nuclear Engineering (MNE) department.

I was a transfer student from Penn State Berks, and I would like to recognize the help and support of Dr. Jeanne Marie Rose, Dr. Cesar Martinez-Garza, Dr. Azar Eslam-Panah, Dr. Leonard Gamberg, Dr. Alexei Prokudin, Mr. Eli Banta, Mr. Adam Haelsig and Ms. Whitney Imoh. Thanks to all of you, I pursued this honors degree, got involved in research and instilled the willpower in me that was needed to take on such a challenge.

Most importantly, I would like to give special thanks to my family and friends, especially my parents for helping me get to where I am today. Their financial, emotional and mental support was critical to my wellbeing and eventual completion of this thesis as well as the accompanying honors degree.

Chapter 1

Background

1.1 Introduction

Rotary vane expanders are well suited for use as work producing (expander) or delivering (compressor) devices in micro- to small-scale power generation systems, such as domestic Organic Rankine Cycles and work recovery expanders in refrigeration systems [1-4]. The simplicity of the technology, compatibility with various working fluids and lower rotational speed, makes this system desirable in operations where a micro-turbine might not be ideal. Our Penn State research team was tasked with developing a power generating system capable of powering a landed mission on Venus for an extended duration of time. The complexity of our working environment coupled with its flexibility of operating conditions, made the rotary vane expander the most compelling power generating device.

1.2 Motivation: Why Venus?

Developing a power generation cycle for a Venus lander poses challenges due to the hostile environment. The surface pressure is about 90 Earth atmospheres, and the average surface temperature is ~800 Kelvin. These conditions necessitate innovative power generation approaches and preclude the use of conventional working fluids with lower critical points and decomposition temperatures [5-7]. Its atmosphere is mainly Carbon-dioxide along with Nitrogen and Sulfuric acid, then when coupled with the high temperatures and pressures, leads to destructive conditions for many materials [6, 7]. All these conditions lead to significant challenges for material science and systems engineering.

Respectively, Venus's total mass and gravitational density are about 80% and 90% less compared to that of Earth's [6]. Additionally, due to the size and proximity similarities, it is believed that by studying

Venus's atmosphere and its surface, we could offer more information on the development of planets. Specifically, by uncovering the history of Venus, we could gain insights on the possible implications of climate change. The uniqueness of Earth is encapsulated by the fact that Venus and Mars both evolved drastically different environments compared to that of Earth's. It has been hypothesized that the higher temperature of Venus might have originated from a "runaway greenhouse effect of a magnitude seemingly incommensurate with Venus's slightly smaller orbital radius" [5]. Since proximity to the sun has been deemed minor, if not negligible, more research into the atmosphere and the planets volcanic releases is needed to update our predicted impacts of greenhouse gas emissions and climate change.

1.3 Prior Missions to Venus

The Soviet Union's space program made significant progress in the exploration of Venus with its Venera and Vega programs. These programs had a total of 17 trips: 15 through the Venera program and an additional 2 through the subsequent Vega program. Achievements of the Venera program include: first man-made devices to enter another planet's atmosphere (Venera 3 in 1965), first probe to transmit data from the atmosphere of another planet (Venera 4 in 1967), first "soft landing" of a craft (Venera 7 in 1970), first craft to transmit data to Earth from the surface of another planet (Venera 7 in 1970), and first mission to capture an picture a planet's surface (Venera 9 in 1975) [8].

Before these successes came some failures. The first 3 missions all failed due to the extreme Venus environment. The atmosphere of Venus was unknown at that time and the first crafts (Venera 1-3) were designed to withstand pressures up to 5 bars and 80°C; thus, they succumbed to the hostile environment. Venera 4-6 were designed for 300°C because that was the believed surface temperature of ~500°C. Most crafts that successfully made it to the surface lasted about 50 minutes, but the most successful was Venera 13 which lasted 127 minutes and transmitted 14 colored and 8 black and white photographs.

1.4 Objective

Due to the limited exploration time of landed Venus missions, our Penn State research team has been tasked with developing a demonstration-scale power generation system that can meet the power requirements of an extended landed mission to Venus (over 100 hours). This system would deliver both electrical power and mechanical work to drive a refrigerator for craft cooling. This study focuses on modeling and analyzing the performance of the selected expansion device: the rotary vane expander.

Several models of rotary vane expanders have been proposed by researchers, focusing on different applications and aspects of the technology. However, all models have been focused on 'Earth-Compatible Systems' such as Organic Rankine Cycles or regeneration of energy in a refrigeration system by replacing the throttling/expansion device with a work delivering rotary vane expander. By developing a dynamic model of a RVE that is adaptable to various working conditions and compatible with new working fluids (*e.g.*, mercury), we could predict and generate a performance matrix tool for variables such as power output, pressure ratio, torque, and RPM.

The modeled rotary vane expander would be part of a Rankine power cycle that was proposed for a landed mission to Venus. The hostile environment of Venus necessitates new working fluids with critical points above the ambient conditions (*e.g.*, iodine, sulfur, mercury). With this model, we will be able to design a rotary vane expander to meet torque, power output, and efficiency goals for the mercury Rankine cycle. Additionally, we expect the data from the eventual model validation efforts to add to the technical community's performance matrix of rotary vane expanders.

1.5 Overview of the Power System

As mentioned earlier, designing a power system for Venus has numerous challenges due to the corrosive atmosphere, high temperatures, and pressures. Most traditional internal combustion gas power cycles such as the Brayton, Otto, and Diesel cycles which require combustion of fuel within the working fluid would not be feasible in this oxygen deficient environment [7]. Moreover, closed gas cycles would be impractical on Venus because they typically operate at temperature ratios greater than 2-3 relative to the ambient conditions. Therefore, we have chosen the Rankine cycle because it is a closed-vapor cycle that is flexible with working fluids while being less reliant on the ambient conditions it operates in.

With the Rankine power cycle selected, a compatible working fluid needed to be chosen. The ambient temperature on Venus is above the critical temperature of conventional power cycle working fluids [9] (*e.g.*, water, organic working fluids), preventing their use. Therefore, for this proposal, we selected mercury as the most suitable working fluid based on its critical point. Additional studies conducted by NASA in 1969, have demonstrated the feasibility of a mercury Rankine power cycle [10].

The next step in the power system design was to select an appropriate heat source and cooling/condensing approach. With limited oxygen on the surface of Venus [7], traditional heat sources such as combustion of hydrocarbons are not feasible. Due to low availability of plutonium, a nuclear-powered source is also not feasible. Solar intensity is not sufficient for power generation due to the dense atmosphere [6, 7, 9]. Current battery technologies cannot operate at these temperatures (and acidic atmosphere), and the low energy density of most batteries technologies would lead to unacceptable flight weights. This led our research group to explore more unconventional heat sources, such as the in-situ resource utilization of the high levels of CO_2 in the atmosphere for other forms of combustion. We selected a Li-CO_2 combustor that effectively uses the ambient CO_2 in the atmosphere to react with the onboard lithium (fuel source), thereby generating up to 12.3kWth at a variable rate (See Figure 1).

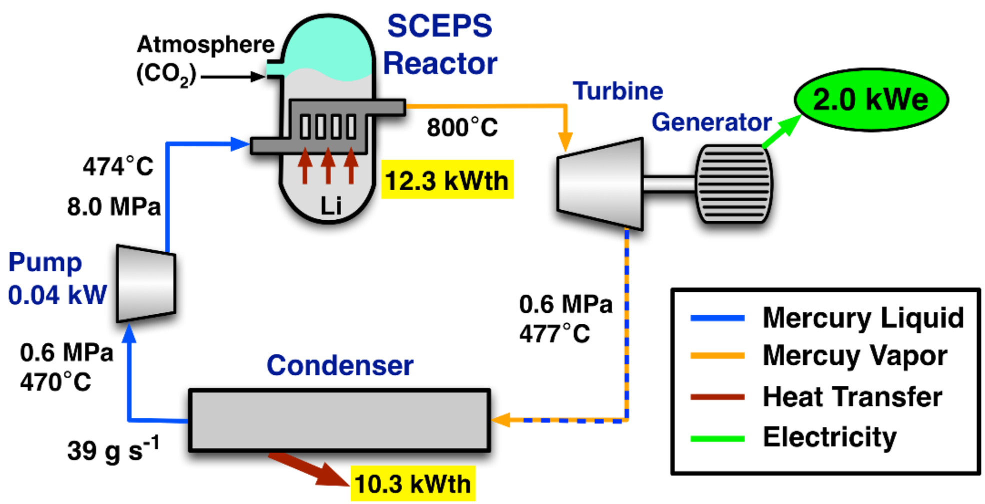

Figure 1 Diagram of the proposed Power and Cooling System

The last step to complete the system is determining the right devices for the expansion and compression/pumping stages. To meet the power requirements of this system, a durable, robust power generation expander is required due to the harsh intensity of the working environment externally and the working fluid internally. We chose a rotary vane expander due to the simplicity and compatibility with a wide range of operating conditions. The full extent and comparison is detailed and discussed below.

Chapter 2

Literature Review

2.1 Why Rotary Vane Expanders?

Durability and enhanced lifespan were critical targets in this project. This meant that we had to choose a mechanically simple system that had few possible modes of failure. Typically, a modified turbine would be the standard expander type selected for power generation. However, turbines typically operate at high RPMs, with thin blades and require consistent fluid flow streams to run efficiently. These are examples of characteristics that cannot be guaranteed during operations and must be taken into consideration when selecting the desired expander

Given the extreme nature of the working environment, innovative solutions are needed to work with those harsh elements. Those harsh elements necessities a power system that is functional in the two-phase flow, uses low working fluid velocity, has a low revolution speed, is durable and simple, and reasonable in cost while still meeting our proposed power requirement. Table 1 below, shows a detailed comparison of various expanders [1]. The rotary vane expander (RVE), is clearly the most favorable of all the expanders analyzed despite scoring low on the power capability. We can compromise on power capability because of our low power requirement.

Table 1: Comparison of various types of expanders

Expander type	Turbine	Scroll	Screw	Vane	Piston
Power	high/medium	medium/low	medium	low	medium
Working fluid flow velocity	very high	low	medium	low	medium
Technical complication	very high	high	high	low	high
Rotational speed	very high	low	low	low	medium
Noise	high	low	medium	low	high
Operation in wet vapor conditions	no	no	yes	yes	no
Difficulty of air-tight sealing	high	medium	high	low	high
Cost	high	medium	high	very low	medium
Services costs	very high	medium	high	very low	medium
Durability	high	medium	high	medium	medium
Internal mechanical friction	low	medium	medium	medium	high

2.2 Breakdown: How They Work

There are multiple types of RVE such as: Rotary Lobe, Dual Port Elliptic and Micro Multi-Vane Expander (MVE). All three expanders were used in a study by Kolasinski *et al.* [2]. In their study, the Rotary Lobe Expanders was the largest and had the highest power capacity of up to 3 kW. The Elliptic expander could output up to 1.5 kW with its dual inlet (suction) and outlet (discharge) port. Lastly, the micro-MVE had a maximum power output of 300 W [2]. Their micro-MVE meets our system requirements, but the maximum capacity of these expanders scale with size. In this thesis, we will be focused on the micro-MVE due to its simplicity and size requirements for the power system.

A RVE can be divided into three major functional sub-groups: structural, sliding vane, and ports. The structural sub-group refers to all the parts that are used to form the entire enclosure, this includes the: cylinder, rotor, and end caps. The cylinder refers to the stationary, hollowed frame that encloses the whole process; its inner walls could be circular or elliptical. The rotor is typically circular, houses the vanes, and is coupled to the driving shaft. The end caps ensure that leakages through the ends are minimized. The vanes are the compartmentalizers that ensure each rotating chamber maintains its fluid inventory. The vanes must contact the inner walls of the cylinder and this can be achieved by springs loaded in the vane slots, centrifugal force, or fluid pressure. Additionally, the vanes represent the area on which the varying pressure act upon to generate and transmit torque to the rotor. Lastly, the ports refer to the inlet and outlet ports and the seals that can be used to prevent leakages between ports. Their strategic locations greatly affect the performance as it partially determines the expansion and pressure ratios. Figure 2b shows all the parts of a RVE in a clockwise, spring load micro-MVE.

The RVE operates by utilizing the variations in pressure in each working chamber to rotate the eccentric rotor. Each working chamber cycles through the processes of filling, expansion, and discharge. The filling stage is initiated when a working chamber is exposed to the inlet port; the difference in pressure coupled with the mass flow rate at the inlet port, adds high enthalpy working fluid into the control volume.

Then as the rotor rotates and closes off a working chamber, the purely expansion process begins due to the rotor being placed eccentrically to the outer cylinder. As the volume of the working chamber expands and does work, the internal energy of the fluid decreases and thus pressure and temperature decrease while mass stays constant if leakage is neglected. Lastly, the discharge phase doubles as a compression/volume reduction phase in which the outlet port evacuates the working chamber and stabilizes its pressure and temperature while reducing the volume to prepare for the next cycle. This variation in pressure, area and moment arm length induce a force and torque imbalance on the axis of the rotor.

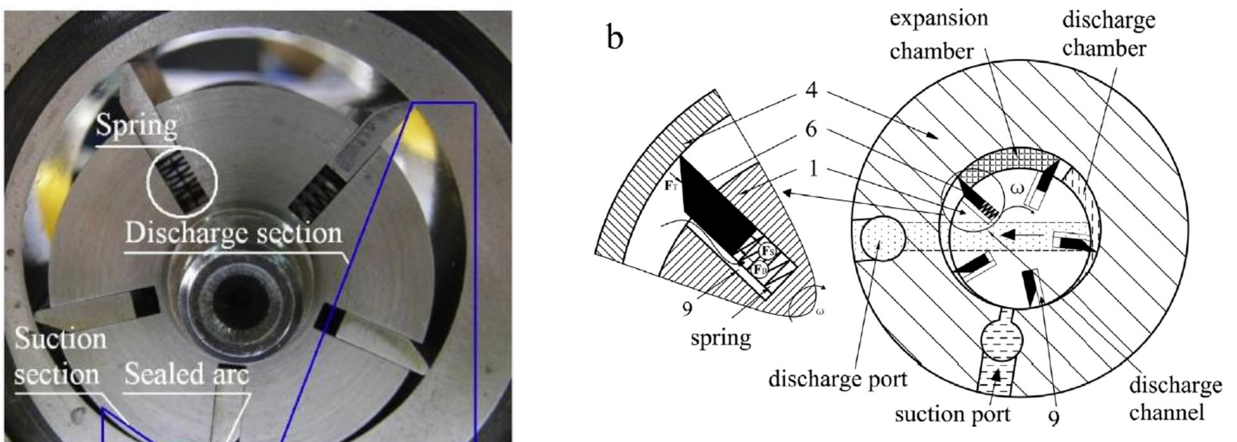

Structure and structure improvement of the sliding vane expander. 1-rotor, 2-left end cap, 3-bearing chock, 4-cylinder, 5-right end cap 6-vane, 7-bearing, 8-sealing groove 9-back-pressure groove.

Figure 2: (a) Image of the internal working of an Eccentric RVE with the inlet and outlet section; (b) Image of the components that make up the RVE. [3]

At every rotational angle, the RVE is designed to have an average net torque due to the differences in pressure in each working chamber. The net torque is used to turn the rotor and driving shaft at a specific rpm to generate power for the system. The cycle is kept consistent by controlling the mass flow rate and the enthalpy of the working fluid entering the working chamber. Several studies focused on the modeling and experimental characteristics of individual operating procedures and their components [2, 4, 11-14]. This literature review focuses on 3 key areas that are particularly relevant to the present study: Leakage Paths, Computational Fluid Dynamics (CFD) and Vane Friction models.

2.3 Prior Assessments on Leakage Paths

No expansion device can achieve ideal performance due to heat loss, friction, and mass leakages. RVEs suffer most of their losses through friction and numerous paths of leakages between working chambers and inlet to outlet ports. Figure 3a shows all five potential leakage paths in an Elliptical RVE, but, these paths are applicable to all forms of RVE. To approach the idealized performance of a RVE, the leakage path of these working fluid must be minimized to increase efficiency. Path 1 shows a direct leakage from the inlet to the outlet port. Path 2 shows a leakage path between two working chambers through the sides of the end caps. Path 3, 4 and 5 show leakage paths between two working chambers over, around and under the sliding vane respectively.

Table 2: List and description of all leakage paths also shown in Figure 3

Leakage Path	Description of Flow Path
Path 1	High enthalpy flow from inlet port directly to the outlet port
Path 2	Flow from a chamber to any other chamber through the end cap
Path 3	Flow over the vane when not in contact with stator wall
Path 4	Flow around the vane through the vane slot gaps
Path 5	Flow around the vane through end cap gaps

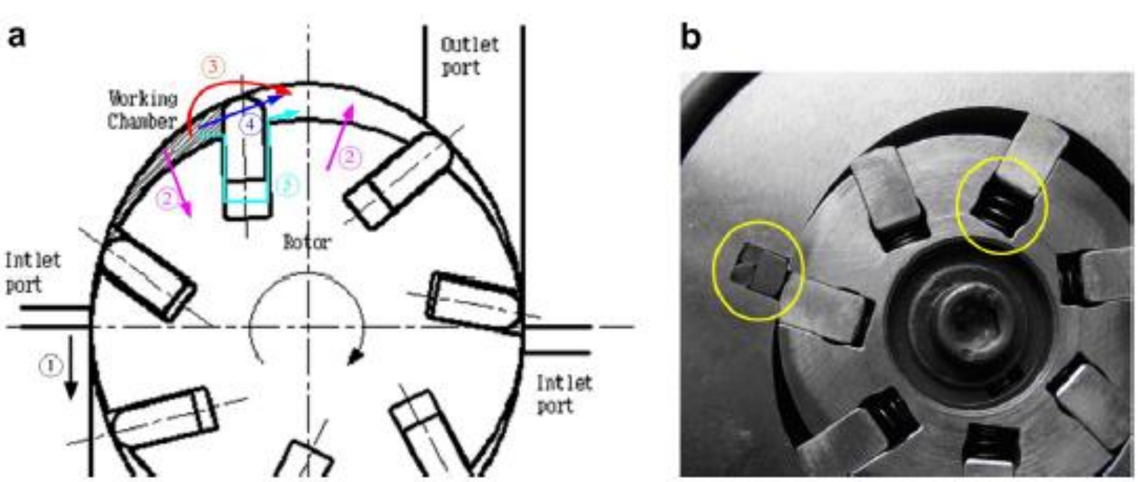

Figure 3: (a) The 5 main leakage paths out of the working chamber (b) Preventative sealing methods [14]

In the study by Yang *et al.*, path 1 and 3 were deemed to be the most significant paths for losses within the RVE [4]. Path 1 leakages were critical because the high enthalpy working fluid being generated completely bypassed the rotor expansion process and went to the outlet port. Figure 3b shows a seal in place to minimize this loss but also resulted in increased work lost due to friction. Additionally, losses through path 3 are dependent on the degree of contact that the vane has on the outer cylinder. In the study of the internal working process, Yang *et al.* found that vanes relying on centripetal and back pressure force alone did not make sufficient contact with the outer cylinder walls (see Figure 4). This loss is significant because, in the event of lost contact, two working chambers could balance out to become one, therefore decreasing the pressure ratio and efficiency of the system. They concluded that a spring was necessary and had to be placed underneath the sliding vane in the vane slot. However, additional work losses were reported due to friction as the spring in complete compression resulted in a high normal force between the vane and the cylinder, which is proportional to frictional force.

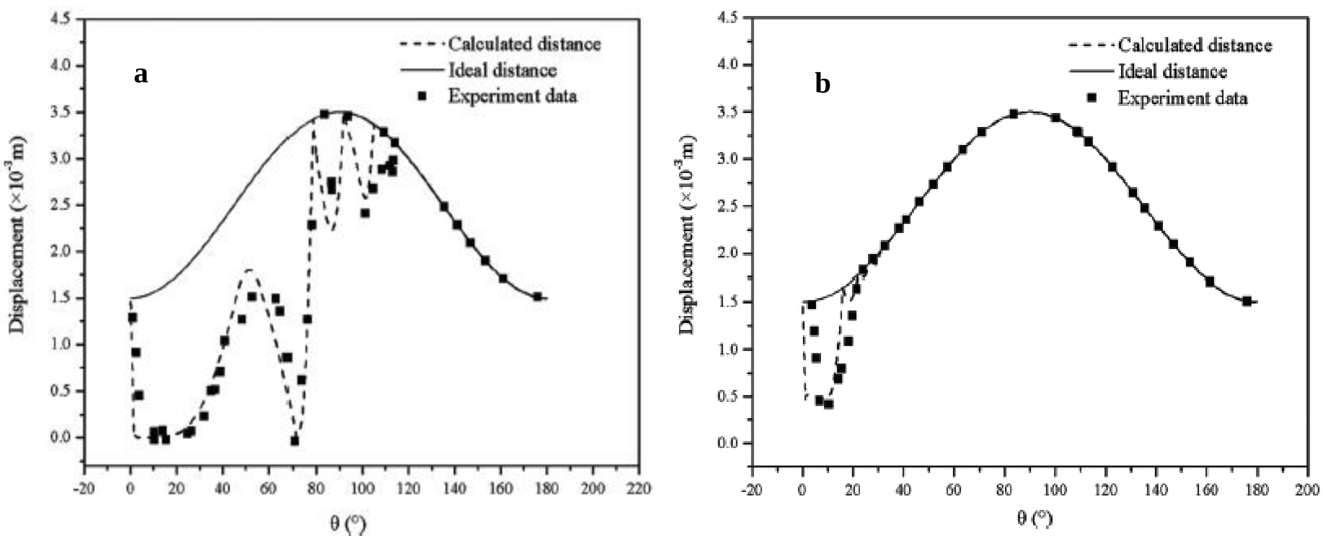

Figure 4: Vane movement in the slot where (a) represents the vane movement without the spring and (b) represents the vane movement with the spring [4]

2.4 CFD Modelling

There have been numerous attempts to model the performances of a rotary vane while taking these mass losses due to leakage into consideration. Kolasinski *et al.* utilized a 3D CFD program at set angles to visualize the fluid losses in an Organic Rankine Cycle using R123 refrigerant [2]. Figure 5 and Figure 6 below shows the results for the temperature and pressure distribution. A key assumption typically made in the modeling of the control volume is equal thermodynamic properties within the control volume; this CFD model result helps verifies this assumption.

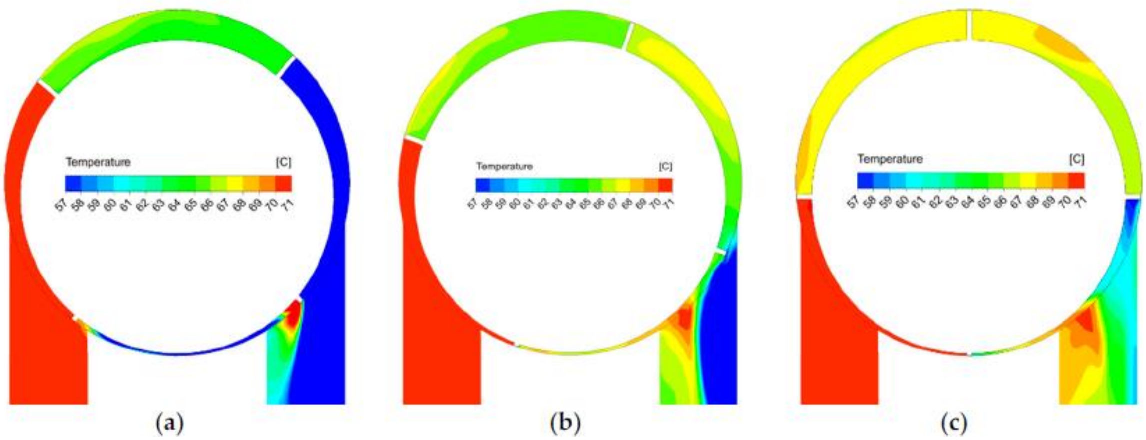

Figure 5: The temperature distribution inside the expander for expansion ratio σ = 4.3 in an ideal gas model at: (a) ϕ=1.50π; (b) ϕ=1.75π; (c) ϕ=2.00π; [2]

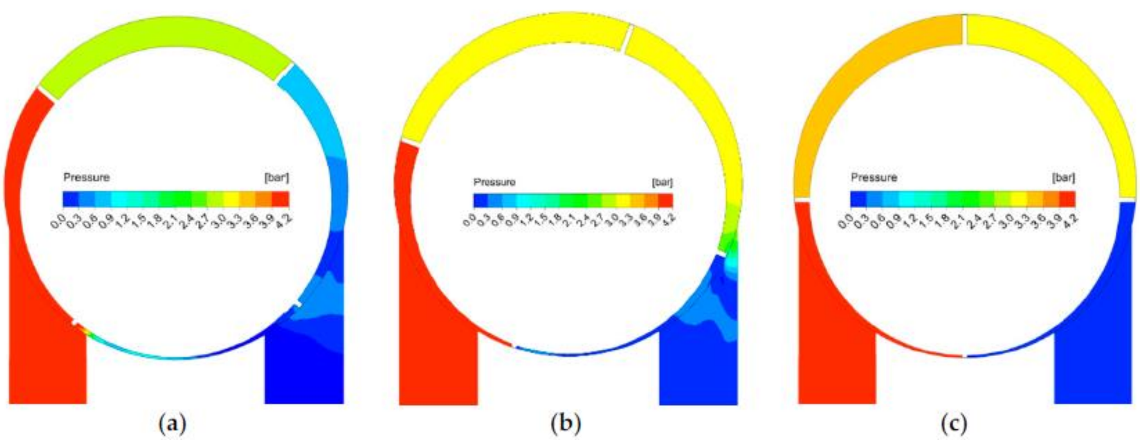

Figure 6: The relative pressure distribution inside the expander of the expansion ratio σ = 4.3 in an ideal gas model at: (a) ϕ=1.50π; (b) ϕ=1.75π; (c) ϕ=2.00π; [2]

2.5 Vane Friction Modelling

Multiple studies by Bianchi and Cipollone [11, 12], focused on modeling the friction power losses as well as the effect of lubrication. Figure 7 shows the detailed free-body force diagram of a vane to assess all the possible vane orientation and sources of friction. This comprehensive model takes the translational, rotational, and fictitious forces such as centrifugal and Coriolis forces, all into consideration and derives a mathematical system of equation for the unknowns. With F1, F2, and F3 being the unknows, they applied Newton's second law in the x and y-axis, as well as a moment equation about the z-axis at F1. Classical mechanics states that with three equations we can solve for the three unknown forces. This 3D problem was simplified to a 2D problem by neglecting forces in the z-axis as well as rotations about the x and y-axis due to the tight tolerances these devices typically have to minimize leakages. Additionally, this study did not account for spring-loaded vanes as F_{spring} will also vary with compression distance.

Newton's second law for the forces at equilibrium in the x-axis ($\sum F_x = m\overrightarrow{a_x} = 0$)

$$F_1 - F_2 - k_2F_3 = F_{pn} - F_{cor} + k_4F_c \tag{1}$$

Newton's second law for the forces at equilibrium in the y-axis ($\sum F_y = m\overrightarrow{a_y} = 0$)

$$k_1F_3 - \lambda F_1 - \lambda F_2 = F_{in} + k_3F_c \tag{2}$$

Newton's second law for the moments at F1 in the z-axis ($\sum M_z = I\overrightarrow{\alpha_z} = 0$)

$$F_2\big(\lambda t_{bl} - (L_{bl} - L_{out})\big) + F_3\left(k_2L_{out} - k_1\frac{t_{bl}}{2}\right) \tag{3}$$

$$= F_c\left(k_4\left(\frac{l_{bl}}{2} - L_{out}\right) - k_3\frac{t_{bl}}{2}\right) - F_{pn}\frac{L_{out}}{2} - F_{in}\frac{t_{bl}}{2} - F_{cor}\left(\frac{L_{bl}}{2} - L_{out}\right)$$

The combined set of equations 1-3 in matrix form is:

$$\begin{pmatrix} 1 & -1 & -k_2 \\ -\lambda & -\lambda & k_1 \\ 0 & \lambda t_{bl} - (L_{bl} - L_{out}) & k_2L_{out} - k_1\dfrac{t_{bl}}{2} \end{pmatrix}\begin{pmatrix} F_1 \\ F_2 \\ F_3 \end{pmatrix} \tag{4}$$

$$= \begin{pmatrix} F_{pn} - F_{cor} + k_4F_c \\ F_{in} + k_3F_c \\ F_c\left(k_4\left(\dfrac{l_{bl}}{2} - L_{out}\right) - k_3\dfrac{t_{bl}}{2}\right) - F_{pn}\dfrac{L_{out}}{2} - F_{in}\dfrac{t_{bl}}{2} - F_{cor}\left(\dfrac{L_{bl}}{2} - L_{out}\right) \end{pmatrix}$$

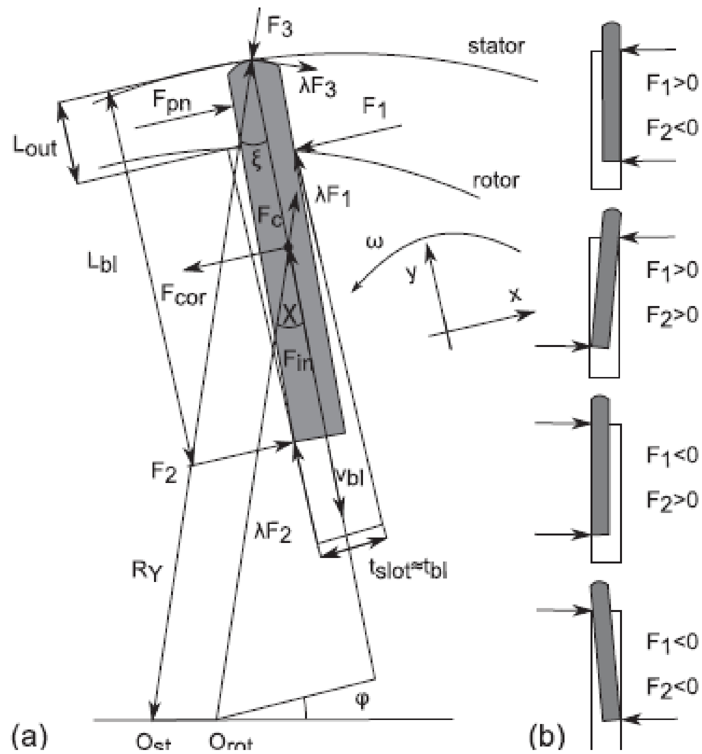

Figure 7: Blade dynamics – (a) free body diagram and (b) possible blade arrangements inside the rotor slot [12]

By solving for F1-3, they were able to calculate the "overall friction power":

$$P_{fr} = \lambda\left(F_3 v_{tip} + v_{bl}(F_1 + F_2)\right)$$

These studies all took a different approach to modeling the RVE, however, none of these models focused specifically on using Mercury as the working fluid. As such, we needed to derive a thermodynamic model of this system to confirm the power capabilities of using any fluid as our working fluid. These individual studies and their results would need to be compounded into a comprehensive model using assumptions that have already been verified in those studies.

Chapter 3

Deriving the theoretical model:

The Penn State research team needed a means of determining the RVE performance in a proposed Venus Lander. This model should be versatile enough to support the working fluid for the preliminary test (such as Argon and Air) and more complex working fluids such as the proposed Mercury. Additionally, as the team is in the design phase of the project, they required a dynamic model that could accept variations in geometry, total number of vanes and all operational conditions (RPM, pressures, temperature, mass flow rate).

3.1 Assumptions

The following assumptions were adopted, based on prior validated publications [1-4, 11-14]:

1. Heat Transfer was ignored
2. Kinetic and Potential energy of the fluid was ignored
3. Neglected transient/initial variations between working chambers
4. Rotational speed was assumed to be steady
5. Properties of inlet and outlet ports were steady
6. Properties in each chamber were constant (averaged) throughout the volume
7. Seal placed between the ports but friction due to seal neglected
8. Both the rotor and stator (cylinder) are circular
9. Ideal gas law assumed for pressure and density calculation

3.2 Derivation of Thermodynamic Equations

The considered control volume is formed between a pair of vanes (Figure 3a and Figure 8b). At any moment there could be flow from the inlet, to the outlet, leakages between chambers, and expansion or compression. Since kinetic, potential and heat transfer are neglected, the means stated above are the only means of energy change within the control volume. With our assumptions made, control volumes drawn and changes in energy confirmed, we began our derivation for the conservation of energy.

$$\frac{dE_{system}}{dt} = \frac{dU_{cv}}{dt} = (\dot{W}_{in} + \dot{m}_{in}h_{in}) - (\dot{W}_{out} + \dot{m}_{out}h_{out}) \tag{5}$$

Expressing equation (5) in terms of temperature, we get equation (6) below. However, m_{cv} is not a constant and so a product rule had to performed on the left had side of the equation to isolate the time derivative of temperature.

$$\frac{d(m * c_v T)_{cv}}{dt} = (\dot{W}_{in} + \dot{m}_{in}c_p T_{in}) - (\dot{W}_{out} + \dot{m}_{out}c_p T_{cv}) \tag{6}$$

$$c_v \frac{d(m * T)_{cv}}{dt} = c_v \left[T_{cv}\frac{dM_{cv}}{dt} + M_{cv}\frac{dT}{dt}\right] \tag{7}$$

$$\frac{dT_{cv}}{dt} = \left[\left(\dot{W}_{in} + \dot{m}_{in}c_p T_{in}\right) - \left(\dot{W}_{out} + \dot{m}_{out}c_p T_{cv}\right) - \left(c_v T_{cv}\frac{dM_{cv}}{dt}\right)\right] * \frac{1}{c_v M_{cv}} \tag{8}$$

Equation (8) is our final general equation for the entire control volume. $\dot{W}_{in}$ & $\dot{W}_{out}$ refer to the work done by compression and expansion respectively. However, a single control volume cannot simultaneously expand and contract at a given moment in time. Similarly, with reasonable port positioning or the implementation of a sealed arc as seen in Figure 2, there should never be a moment of inlet flow from the high pressure hot section and the low pressure cold section in the same control volume. Therefore, this equation can be further simplified for each stage of the RVE cycle.

The inlet port is positioned during the onset of the expansion process. Therefore, during an open inlet port and expanding control volume, equation (8) simplifies to:

$$\frac{dT_{cv}}{dt} = \left[\dot{m}_{in}c_p T_{in} - P_{cv}\frac{dV}{dt} - \left(c_v T_{cv}\frac{dM_{cv}}{dt}\right)\right] * \frac{1}{c_v M_{cv}} \tag{9}$$

When all the ports are closed to the control volume, it can either be expanding or compressing. The sign of $\frac{\mathrm{dV}}{\mathrm{dt}}$ signifies which process is occurring for each control volume at every moment. Furthermore, we initially assume no leakage between chambers, we set $\frac{d\mathrm{M_{cv}}}{\mathrm{dt}} = 0$. Equation (8) simplifies to:

$$\frac{dT_{cv}}{dt} = \left[-P_{cv}\frac{dV}{dt}\right] * \frac{1}{c_v M_{cv}} \tag{10}$$

Lastly, when the outlet is opened to the control volume and compressing. Note that T_{out} is T_{cv} because that is the temperature of the fluid flowing out of the control volume:

$$\frac{dT_{cv}}{dt} = \left[-\dot{m}_{out}c_p T_{cv} - P_{cv}\frac{dV}{dt} - \left(c_v T_{cv}\frac{dM_{cv}}{dt}\right)\right] * \frac{1}{c_v M_{cv}} \tag{11}$$

3.3 Conservation of Mass

The extra terms such as mass flow rate, volume and pressure were calculated prior to the implementation of equation (8). Since the RVE is an open system, the conservation of energy equation can be coupled with the conservation of mass equation:

$$\frac{dM_{cv}}{dt} = \dot{m}_{in} - \dot{m}_{out} \tag{12}$$

However, just like with our generalized thermodynamic equation for temperature $\left(\frac{dT_{cv}}{dt}\right)$, mass flow rate of the control volume is dependent on the location of the working chamber. With our 1st model's assumption of no leakage between working chambers, we know that $\dot{m}_{in}$ & $\dot{m}_{out}$ correspond to the rate of mass flow at the inlet and outlet port respectively.

Chamber at Inlet Port:	Chamber Closed off:	Chamber at Outlet Port:
$\frac{dM_{cv}}{dt} = \dot{m}_{in}$	$\frac{dM_{cv}}{dt} = 0$	$\frac{dM_{cv}}{dt} = -\dot{m}_{out}$

Realistically, as more fluid flows into the lower pressure control volume, the pressure raises and so the mass flow rate will decrease until the pressures are equalized. Once the pressures are level, there should be no net flow in or out of either control volumes. To simulate this, the pressure percent difference was used as a multiplier to the constant set mass flow rate of the entire power cycle ($\dot{m}_{sys}$):

Chamber at Inlet Port:

$$\frac{dM_{cv}}{dt} = \dot{m}_{sys} * \frac{P_H - P_{cv}}{P_H}$$

Chamber Closed off:

$$\frac{dM_{cv}}{dt} = 0$$

Chamber at Outlet Port:

$$\frac{dM_{cv}}{dt} = -\dot{m}_{sys} * \frac{P_{cv} - P_L}{P_L}$$

Calculating the volume in each working chamber is only a function of the RVE geometry, which is explained in detail below. The last variable that needed to be calculated for the thermodynamic equation for temperature was Pressure. As stated in the assumptions, because of the high temperatures and the type of fluid being used for the validation of this model (air & argon), the ideal gas law was used. So, we determined pressure from the calculated temperature and mass using: $P_{cv} = {}^{M_{cv}\ R\ T_{cv}}/_{V_{cv}}$.

3.4 Volume Integration in Polar Coordinates

The volume of each working chamber is the only property that depends on the geometry of the stator and rotor, as well as the number of vanes. The thickness of the vanes was neglected in our first model. Additionally, as seen in Figure 8a, we are assuming both the rotor and stator are perfect circles with a fixed eccentric distance (e). The next step was to determine the coordinate system for all our geometry calculations. I chose to follow the standard polar coordinate system with counter-clockwise rotation being the positive direction. The origin was selected to be the center of the rotor to future-proof the dimensioning in the event that the stator was not a perfect circle.

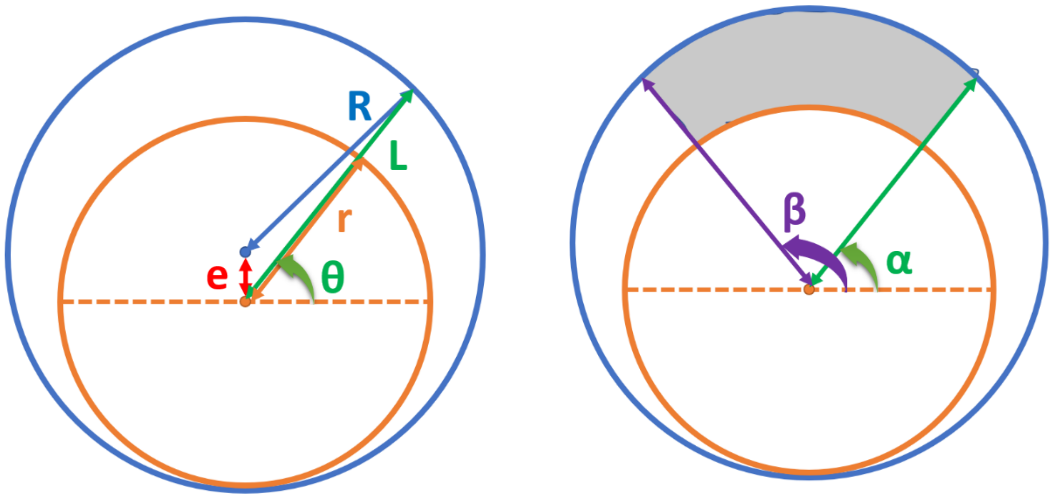

Figure 8: Inner geometric dimensioning: R - Stator radius, r – rotor radius, e – eccentricity, L- Upper integration bound.

To perform an integration in polar coordinates, we need to clearly define the integration bounds (limits) in both the angular theta (θ) and the radial (r) direction. The angular theta bounds were trivial as it went from the current value of $\theta = \alpha$ to $\theta + d_{vane} = \beta$. Figure 8b highlights the angular distance, d_{vane}, between the vanes with α and β being the lower and upper angular integration bound respectively.

$$d_{vane} = \frac{2\pi}{\#\ of\ vanes} \tag{13}$$

Likewise, the radial integration bounds were from the surface of the rotor to the inner wall of the stator. This meant integrating from r to L, but we needed an equation for L in terms of $\theta, R\ and\ e$. Figure 8a shows the triangle formed, ΔeRL. Thus, by applying the laws of sines and cosines and simplifying using trigonometric identities, we derived the final expression for L:

$$L = \sqrt{e^2 + R^2 - \left(2\ e\ R\ \cos\left(90° + \theta - \sin^{-1}\left(\frac{\cos(\theta)\ e}{R}\right)\right)\right)} \tag{14}$$

Since we have all the necessary bounds for our control volume, we calculated the cross-sectional area of the bound by integrating in polar coordinate. The cross-sectional area represented the unit-depth volume of the working chamber when $f(r, \theta) = z = 1$. By applying differential calculus, a differential Area (dA), can be approximated by a rectangle of a differential side length (dr) and differential arc width (dw). Where the differential arc can be approximated by $dw = r\, d\theta$, which stems from the arc equation $s = r\,\theta$. This means that, we can approximate the differential area as: $dA = r\, dr\, d\theta$. Thus, by applying the "Change of Variables", we get the double integral expression:

$$Volume = \iint f(r,\theta) dA = \iint (z)\, r\, dA = \iint (z)\, r\, dr\, d\theta = z \int_{\theta=\alpha}^{\theta=\beta} \int_{r=r_{in}}^{r=L(\theta)} r\ dr\ d\theta \tag{15}$$

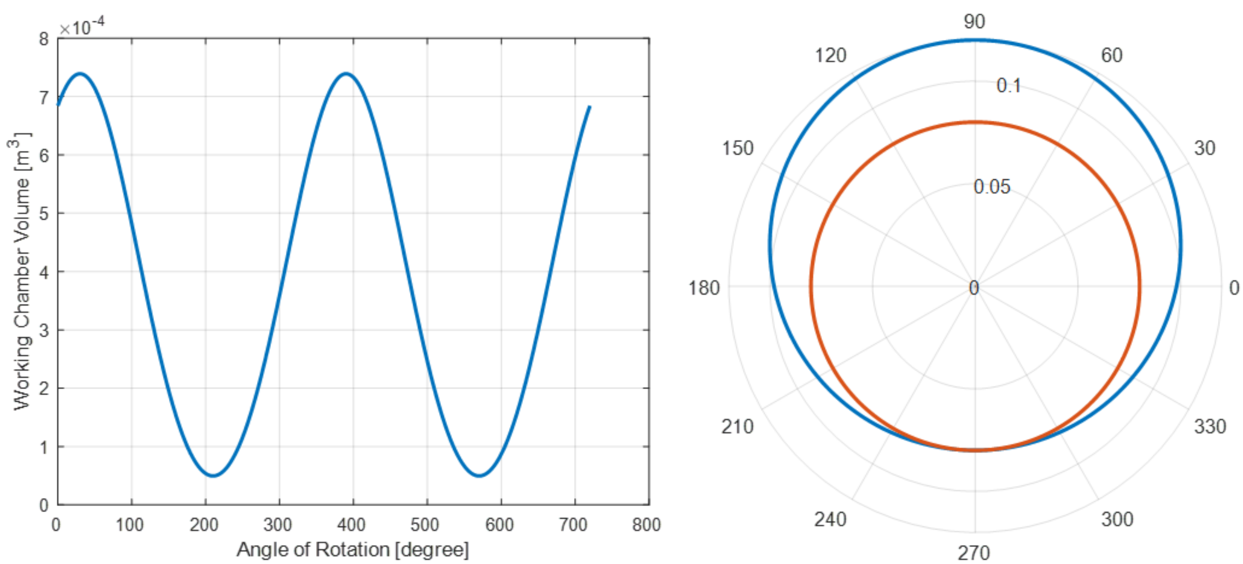

Figure 9: (a) Cyclic volume plot over 2 cycles for a unit depth; (b) Corresponding Geometric plot of rotor and stator when R = 0.1m and e = 0.2*R;

The final variable that our thermodynamic model required was the differential change in Volume with time. Because we only had numeric values for volume with respect to time (equation (15)), a sinusoidal curve fit was used to estimate the volume and volume change rate of each chamber:

$$Fitted\ Volume = amp * sin(freq * V_{time} - phase) + shift \tag{16}$$

$$Fitted \frac{dV}{dt} = freq * amp * cos(freq * V_{time} - phase) \tag{17}$$

Lastly, a vertical shift up ensured the minimum values matched up. Volume could never reach zero. Figure 10 shows the close agreement between the exact results for V and $\frac{dV}{dt}$ and the sinusoidal curve fits, with 6.5% and 13.5% average errors, respectively.

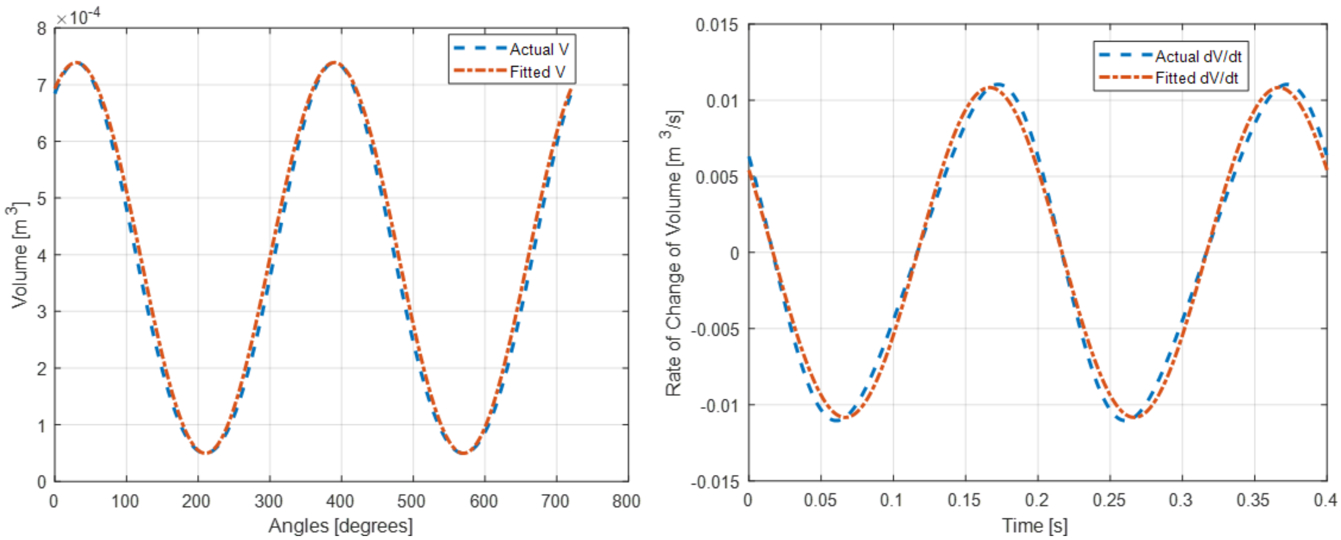

Figure 10: Comparison of the estimated sinusoidal volume function to both the actual volume model and the time-derivative of the volume model

3.5 Friction Related Power and Torque Losses

As discussed in section 2.3 Prior Assessments on Leakage Paths, minimizing leaks between chambers is necessary to ensure that a RVE operates efficiently. Yang [14] suggested using a spring to ensure good contact between the vane tip and the inner wall of the stator. This also implies that there will be friction and thus a trade-off must be made between the strength of the spring and torque/power lost due to friction. We used a simple friction model to estimate the frictional force on each vane [15].

$$F_{friction} = \mu_k * F_{normal} \tag{18}$$

Equation (18) is a standard equation, but the challenge was reasonably estimating the normal force each vane might perceive in a non-symmetric rotating system. Section 2.5 Vane Friction Modelling, summarized the detailed vane dynamic model derived by Bianchi and Cipollone [12], but in our model, by order of magnitude analysis, we simplified the forces acting on vane to centripetal and the spring forces.

$$F_{spring} = -k * x = k * d_r \tag{19}$$

$$F_{centripetal} = m * \overrightarrow{v_t}^2 / r_c \tag{20}$$

Where, $\overrightarrow{v_t}^2 = \omega * r_c$

The spring force (equation (19)) is based on Hooke's law and "d_r" refers to the total compression displacement of the spring due to the sliding of the vane into the vane slot [15]. This resulted in a sinusoidal shape for the spring force as seen in Figure 11. Additionally, the centripetal force also varied in a sinusoidal pattern due to both the tangential velocity $(\overrightarrow{v_t})$ and the radial distance of the vane's center of mass (r_c). Both components, $\overrightarrow{v_t}$ and r_c have radial components in them that vary with every degree of rotation. Lastly, for the mass of the vane (m), we assumed a solid vane homogenously made from SS-316.

Figure 11 illustrates the sinusoidal variations between the spring and the centripetal forces at each angle of rotation. The oscillations of the two forces are opposite, as the peaks of the spring force occurs at the troughs of the inertial force and vice versa. This is because the spring has its peak force when the spring is most compressed; this coincides with the point where of the vane's center of mass (r_c) is smallest.

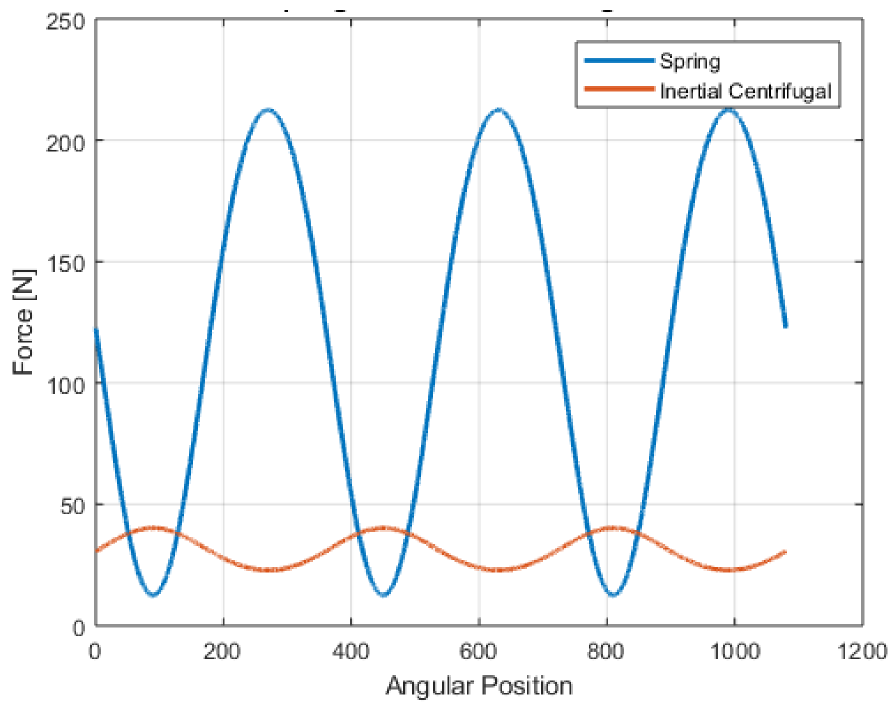

Figure 11: Sample Plot of Spring and Inertial Centrifugal Normal Forces.

For: $m = 0.44\ kg,\ k = 5000\ Nm^{-1}, and\ \omega = 300\ rpm$

The final step in the frictional power and torque losses was to use the combined centripetal and spring force as the total normal force in equation (18) and then calculate the expected losses. Both power and torque are related and are critical engine performance metrics needed during model validation. A full vane dynamic model, detailed in section 2.5 Vane Friction Modelling, would need to be performed to minimize the spring mechanical properties while ensuring the vane tip maintains contact with the stator. Thereby, minimizing the friction and leakage losses which are key to improving engine performance.

$$\text{Power loss: } P_{loss} = \tau_{loss} * \omega \tag{21}$$

$$\text{Torque loss: } \tau = r_{tip} \times F_{friction} = r_{tip} * F_{friction} \tag{22}$$

As torque is dependent on the radial distance of the vane's tip (r_{tip}) and the frictional force, both of which already varied in a sinusoidal manner, our torque and power loss also varies in a sinusoidal manner. The impact of the varying moment arm is seen in Figure 12, as the peaks have smoother and more gradual crests while the troughs are sharper and more sudden.

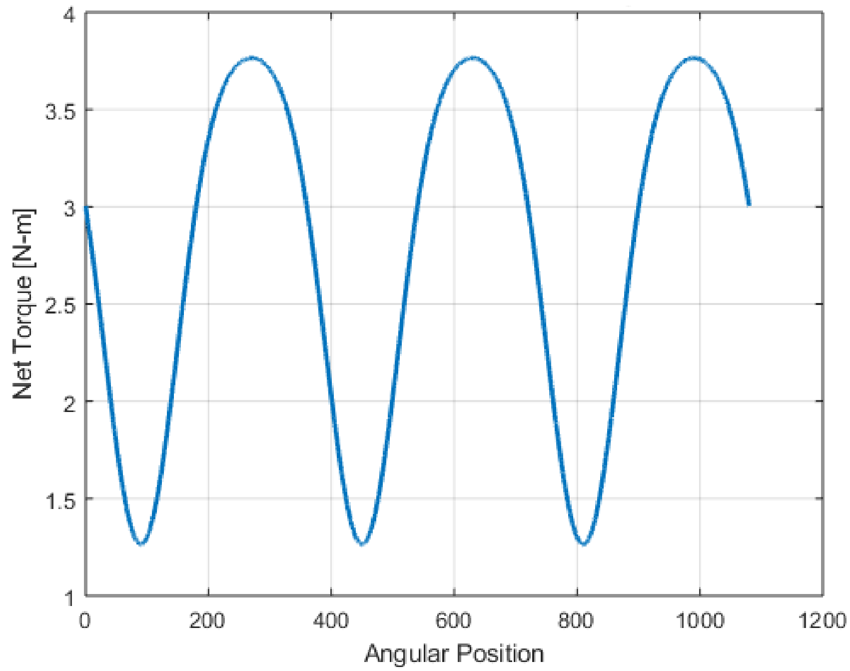

Figure 12: Frictional Torque on a Single Vane Based on Forces in Figure 11

Moreover, Figure 13 shows the total frictional torque and power losses for all the vanes combined. For these sample plots, we see that the net power and torque oscillate at a higher frequency over 3 complete revolutions. However, the overall variations in both plots are minuscule.

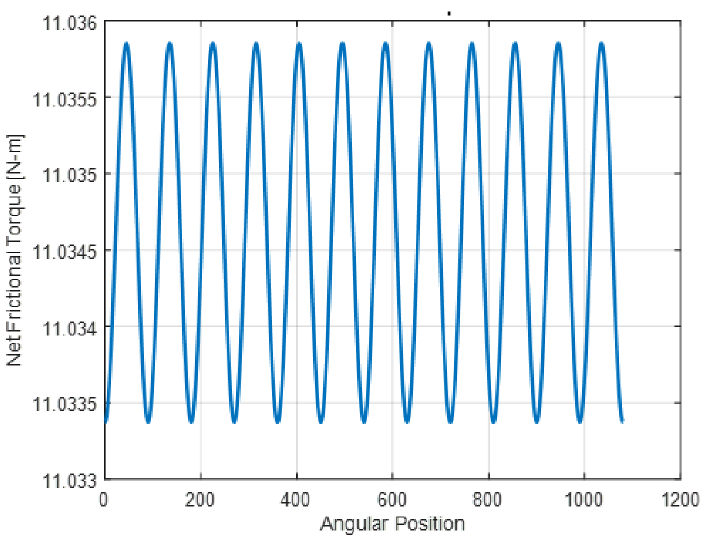

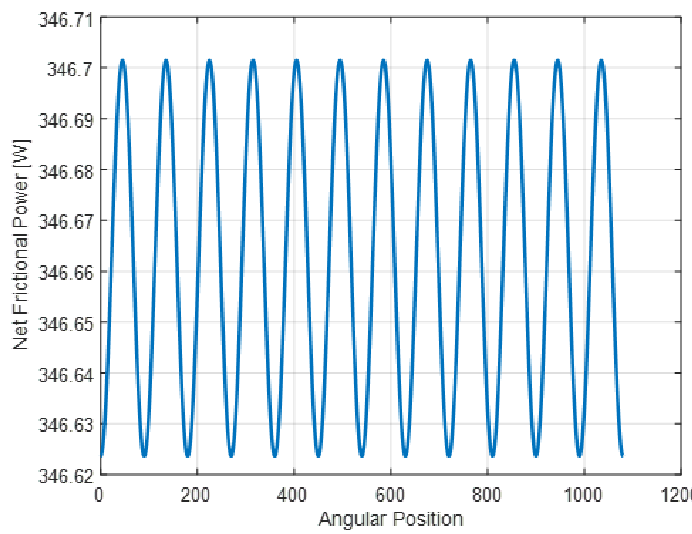

Figure 13: Sample Plot of the Net Torque and Power Losses Due to Friction.

For: $\# \; of \; Vanes = 4, \mu_k = 0.2$

3.6 Mass Leakage Losses

From section 3.5 Friction Related Power and Torque Losses, we see that the only surface which we assumed to have perfect contact was the vane tips sliding across the face on the inner-walls of the stator. Additionally, in section 2.3 Prior Assessments on Leakage Paths, we discussed all the possible leakage paths based on Figure 3. Yang *et al*. [14] showed that leakage path 1 and 3 could be minimized by a seal and a spring respectively, and thus, we neglected them. Path 2 would have been the most complicated to model as it allows for all chambers to simultaneously leak into each other based on their pressures. Fortunately, path 2 would also have been the longest path, thereby restricting the key fully developed assumption and increasing the head loss of any possible flow; thus, we neglected path 2 as well. Path 4 and 5 represent the leakage flow around and under the vane itself. Since path 4 is the shortest path and the path of least resistance, by the order of magnitude analysis, we chose to neglect path 5.

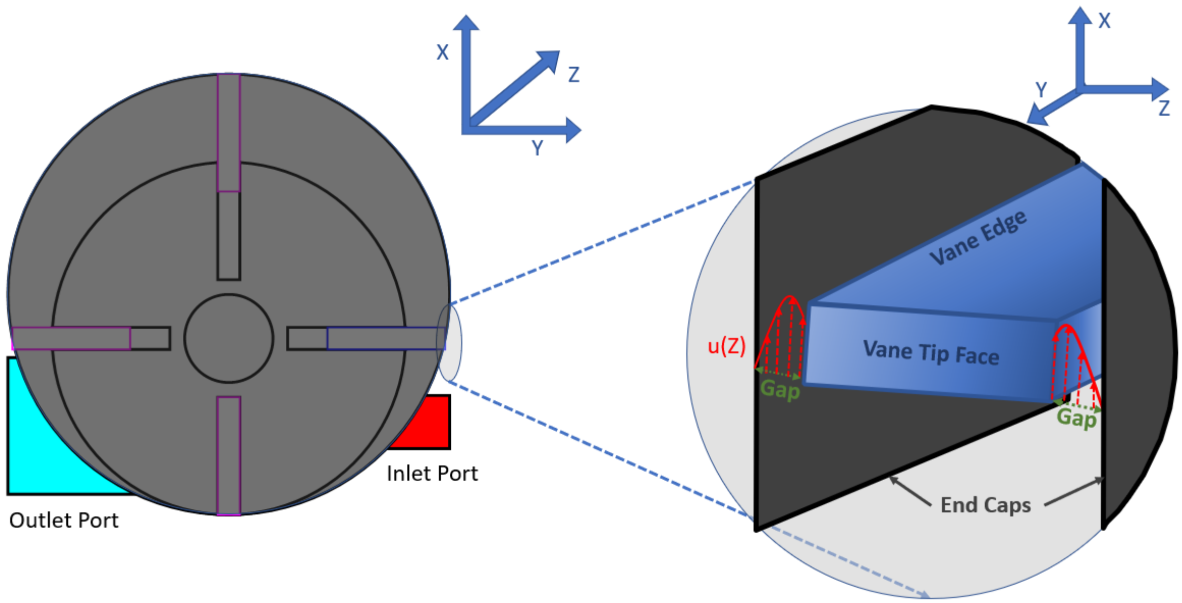

Figure 14: Graphic depiction of leakage flow path and integration axes

Modeling the leakage around the vane edge (path 4) would allow us to increase the accuracy of our model as it was deemed a relevant leak source that is hard to limit due to unwanted friction. Figure 14, shows the slight gap on each side of the vane where the leakage would occur. This gap should be designed into the manufacturing or the vane to reduce contact between the side of the vane and the end caps. Therefore, this gap could be the manufacturing tolerance, manufacturing error and the eventual eroding of material due to wear & tear.

The flow direction is in the x-axis only (azimuthal), but in a single cross-section, the velocity profile only varies in the z-axis (axial); hence ‘u(Z)’. However, the tangential velocity of the vane varies in the y-axis (radial) direction. Thus, the velocity profile is a function of ‘Z’ and ‘Y or r’ (i.e. $\vec{u}(Z,Y) = \overrightarrow{v_\theta}(Z,r)$). Since this is a rotating system, the ‘X’ and ‘Y’ axis would have to rotate with it, so switching to cylindrical coordinates is ideal. ‘X’ and ‘Y’ respectively become, ‘tangential’ and ‘radial’, while ‘Z’ remains the same.

To solve for this velocity flow profile, we must solve the Navier-Stokes Equation (NSE) which is shown in its abbreviated form below as Equation (23). This is a pressure driven flow with shearing due to the end-cap walls being stationary while the vane sides rotate.

$$\rho \frac{D\vec{V}}{Dt} = -\nabla P + \rho \vec{g} + \mu \nabla^2 \vec{V} \tag{23}$$

By expanding Equation (23) and assuming that the leakage process is steady and fully developed, we can set the material derivative $\left(\frac{D\vec{V}}{Dt}\right) = 0$; thereby making the LHS zero as seen in Equation (24)

$$0 = -\frac{1}{r}\frac{\partial P}{\partial \theta} + \rho g_\theta + \mu\left[\frac{\partial}{\partial r}\left(\frac{1}{r}\frac{\partial}{\partial r}(r v_\theta)\right) + \frac{1}{r^2}\frac{\partial^2 v_\theta}{\partial \theta^2} - \frac{2}{r}\frac{\partial v_r}{\partial \theta} + \frac{\partial^2 v_\theta}{\partial z^2}\right] \tag{24}$$

The NSE is a momentum-based expression of Newton’s second law for a fluid body, thus there must be an expression for each axis. Equation (24) is the momentum expression in the θ-direction. We are assuming that the fluid does not flow into the radial nor axial directions; thus, we can neglect both equations. To derive an analytic expression for the leakage velocity profile, we must first generate a single expression in a single cross-section. Figure 14 depicts a single cross-sectional velocity profile which we expect to see in the leakage gap. This singular expression for the tangential velocity profile is a function of ‘Z’ alone (i.e. $\overrightarrow{v_\theta}(Z)$). By neglecting the impact of gravity and canceling out all partial derivatives in terms of ‘r’ and ‘θ’, we get a simplified and solvable expression of the NSE equation (25).

$$\frac{\partial P}{\partial \theta} = r\frac{\partial^2 v_\theta}{\partial z^2} = \frac{\partial^2 \omega r}{\partial z^2} = \frac{\partial^2 \vec{u}}{\partial z^2} \tag{25}$$

Integrating the simplified NSE (equation (25)) twice, results in the analytic expression for the velocity profile, $\vec{u}(z)$, for any cross-section, which is shown below:

$$u(z) = \frac{z^2}{2\mu}\frac{\partial P}{\partial x} + c_1 z + c_2 \tag{26}$$

$$\frac{\partial P}{\partial x} = \frac{P_2 - P_1}{vane\ width}$$

The next step to solving the leakage rate was to determine the boundary conditions on the derived analytic expression for the velocity profile. Based on the pre-defined leakage path (path 4) and the operating conditions of the RVE, we know that our boundary conditions must be: $u(z = 0) = 0$ and $u(z = gap) = \omega r$. Where $z = 0$, represents the end cap which is always stationary, and $z = gap$, represents the edge surface of the vane. By applying the "No-Slip" conditions, we know that $c_2 = 0$ while c_1 is solved below:

$$u(z = gap) = \omega r = \frac{gap^2}{2\mu}\frac{\partial P}{\partial x} + c_1 * gap \tag{27}$$

$$c_1 = \frac{\omega r}{gap} - \frac{gap}{2\mu}\frac{\partial P}{\partial x} \tag{28}$$

Combining equations (26) and (28), we get the full expression for the velocity profile with variables that can be integrated to solve for an analytic solution:

$$u(z) = \frac{z^2}{2\mu}\frac{\partial P}{\partial x} + \left(\frac{\omega r}{gap} - \frac{gap}{2\mu}\frac{\partial P}{\partial x}\right) z \tag{29}$$

The derived velocity profile, $u(z)$, is a 1-dimensional expression. However, we know that in each cross-section, the velocity profile will change and this needs to be account for. From classical fluid dynamic, the flow rate through a gap through the equation: $\dot{m} = \rho\vec{V}A$. Breaking this down, the area term 'A', is refers to the inlet area perpendicular to the leakage flow profile. That is a plane which sits in the radial and 'Z' axis. Integrating $u(z)$ in the z-axis to determine the mass flow rate for a unit depth ($\dot{m}'$). Then by integrating the $\dot{m}'$ expression in a r-axis, we get the total leakage flow rate ($\dot{m}$).

$$\dot{m}' = \rho_{avg} \int_{z=0}^{z=gap} u(z)dz \tag{30}$$

$$\dot{m} = \int_{r_1}^{r_2} \dot{m}'dr = \rho_{avg} \int_{r_1}^{r_2} \int_{z=0}^{z=gap} u(z)dz\,dr \tag{31}$$

The average density was used to simplify the computation for the code, as the density of the fluid in the adjacent compartments could be noticeably different due to varying temperature and pressure. Additionally, the leakage direction does vary during a cycle further complicating the simulation. We opted to compute the analytic expression rather than use the built-in MATLAB integral function to increase the speed of the simulation. The simplified result is shown below in equation (33).

$$\dot{m} = \rho_{avg} \int_{r_1}^{r_2} \left[\frac{gap^3}{6\mu}\frac{\partial P}{\partial x} + \left(\frac{\omega r}{gap} - \frac{gap}{2\mu}\frac{\partial P}{\partial x}\right)\frac{gap^2}{2}\right] dr \tag{32}$$

$$\dot{m} = \rho_{avg}(r_2 - r_1)gap\left[\frac{3\omega\mu(r_2 + r_1) - gap^2\,\frac{\partial P}{\partial x}}{12\mu}\right] \tag{33}$$

With the analytically solved expression for leakage path 4, the assumptions made in the original thermodynamic equations (Equations (9)-(11)) derived in section 3.2 Derivation of Thermodynamic Equations, must be modified to account for leakage into and out of the CV. The fluid flowing in changes the energy equations and the mass equations as it adds or removes energy and mass in the process. The updated expressions are listed below for the open inlet, closed ports and open outlet respectively:

$$\frac{dT_{cv}}{dt} = \left[\dot{m}_{in}c_pT_{in} + \dot{m}_{L1}c_pT_{L1} - \dot{m}_{L2}c_pT_{L2} - P_{cv}\frac{dV}{dt} - c_vT_{cv}\frac{dM_{cv}}{dt}\right] * \frac{1}{c_vM_{cv}} \tag{34}$$

$$\frac{dT_{cv}}{dt} = \left[\dot{m}_{L1}c_pT_{L1} - \dot{m}_{L2}c_pT_{L2} - P_{cv}\frac{dV}{dt} - c_vT_{cv}\frac{dM_{cv}}{dt}\right] * \frac{1}{c_vM_{cv}} \tag{35}$$

$$\frac{dT_{cv}}{dt} = \left[-\dot{m}_{out}c_pT_{cv} + \dot{m}_{L1}c_pT_{L1} - \dot{m}_{L2}c_pT_{L2} - P_{cv}\frac{dV}{dt} - c_vT_{cv}\frac{dM_{cv}}{dt}\right] * \frac{1}{c_vM_{cv}} \tag{36}$$

From the new expressions, Equations (34)-(36), $\dot{m}_{L1}$ refers to the leakage flow rate from the previous chamber into the current chamber. $\dot{m}_{L1}$ is not always positive, but since it is always defined as flowing into the current CV, then the sign corrects the equation itself. T_{L1} represents the temperature of the fluid entering or leaving the CV based on $\dot{m}_{L1}$ and its sign. Likewise, $\dot{m}_{L2}$ and T_{L2} are the fluid flow properties between the current chamber and the chamber ahead. $\dot{m}_{L2}$ always has a negative sign before it because it is calculated just like $\dot{m}_{L1}$, but for the chamber ahead; thus, the sign must always be flipped.

Similarly, changes also had to be implemented to the conservation of mass equations. Each CV always had to leakage paths to it adjacent CVs. Below are the updated time derivative of mass expressions for each chamber location, where $\dot{m}_{in}$ and $\dot{m}_{out}$ represent the varying flow rate into and out of the CV:

Chamber at Inlet Port:

$$\frac{dM_{cv}}{dt} = \dot{m}_{in} + \dot{m}_{L1} - \dot{m}_{L2}$$

Chamber Closed off:

$$\frac{dM_{cv}}{dt} = \dot{m}_{L1} - \dot{m}_{L2}$$

Chamber at Outlet Port:

$$\frac{dM_{cv}}{dt} = -\dot{m}_{out} + \dot{m}_{L1} - \dot{m}_{L2}$$

Chapter 4

Model Results:

4.1 Operating Conditions and Pre-Defined Constants

The RVE model detailed in Chapter 3, was implemented as two programs in MATLAB [16]: basic_model_single.m and basic_model_varying.m. basic_model_single.m produces intermediate plots of thermodynamic properties, friction, leakage, torque, and power for each working chamber. basic_model_varying.m, builds on the basic_model_single.m program by transitioning it into an executable function. Thereby, permitting the user to pass through an array of operating conditions. Performance and efficiency plots generated by the second program, are useful for designing and optimizing the fielded RVE.

Table 3 -Table 5 represent the values of the variables set in both the single and the varying program. However, the varying script is capable of varying inlet Pressure, RPM and mass flow-rate. For this paper, we chose to run the code assuming air flow at conventional air motor conditions. In this case, the air exhausts to standard atmospheric conditions (P_L and T_L). It was assumed that the inlet gas was at elevated temperature. Following the findings of Kolasinski and co., we chose to limit the inlet pressure based on the accepted range of pressure ratios ($\sigma = 3 - 10$) [13]. Therefore, our inlet pressure was set to ten times that of standard atmospheric conditions and additionaly matched their RVE geometry.

Table 3: The Working Fluid's Operating Properties

$P_H = 1000$	[kPa] inlet pressure	$m_{flow} = 0.15$	[kg/s] flow rate
$P_L = 100$	[kPa] outlet pressure	$c_p = 1006$	[J/kg-K] for air
$T_H = 350$	[K] inlet temperature	$c_v = 730$	[J/kg-K] for air
$T_L = 298$	[K] outlet temperature	$R_{air} = 276$	[J/kg-K] for air
$\rho = 0.785$	[kg/m^3] air density	$\mu_{air} = 25e\text{-}6$	[kg/m-s] viscosity

Table 4: The RVE Geometric Dimensions and Simulation Port Locations

$R = 0.1$	[m] radius of stator	Vanes = 4	number of vanes
$e = 0.02$	[m] eccentricity	RPM = 300	[rpm] speed
$r = 0.08$	[m] radius of rotor	In = 315:330	[deg.] inlet port
$z = 0.1$	[m] length of rotor	Out = 140:225	[deg.] outlet port
Gap = 0.1e-3	[m] manuf. tolerance	Revs = 3	# of revolutions

Table 5: The Sliding Vane, Spring and Friction Properties

$H_{vane} = 0.055$	[m] Vane Height	$k_{spring} = 5000$	[N/m] stiffness
$W_{vane} = 0.01$	[m] Vane Width	$L_{spring} = 0.0675$	[m] free height
$\rho_{vane} = 8000$	[kg/m^3] SS316 density	$\mu_{friction} = 0.2$	Friction coeff.

4.2 Individual Control Volume Fluid and Thermodynamic Results:

This section focuses on the results of the simulation from all the conditions listed above (Table 3-Table 5), through the first MATLAB program (basic_model_single.m). The initial conditions were set to the ambient or the outlet conditions and run for a total of three revolutions. As you will see later, because we neglected the transient startup of the RVE (where RPM = 0), our system equalizes within 1 revolution. The code simulates the changes in the pressure, mass, and temperature of each CV assuming constant RPM through the ode45 function. Then by storing the outputs of the function (the variation of the three varying fluid properties of each CV), we generated Figure 15

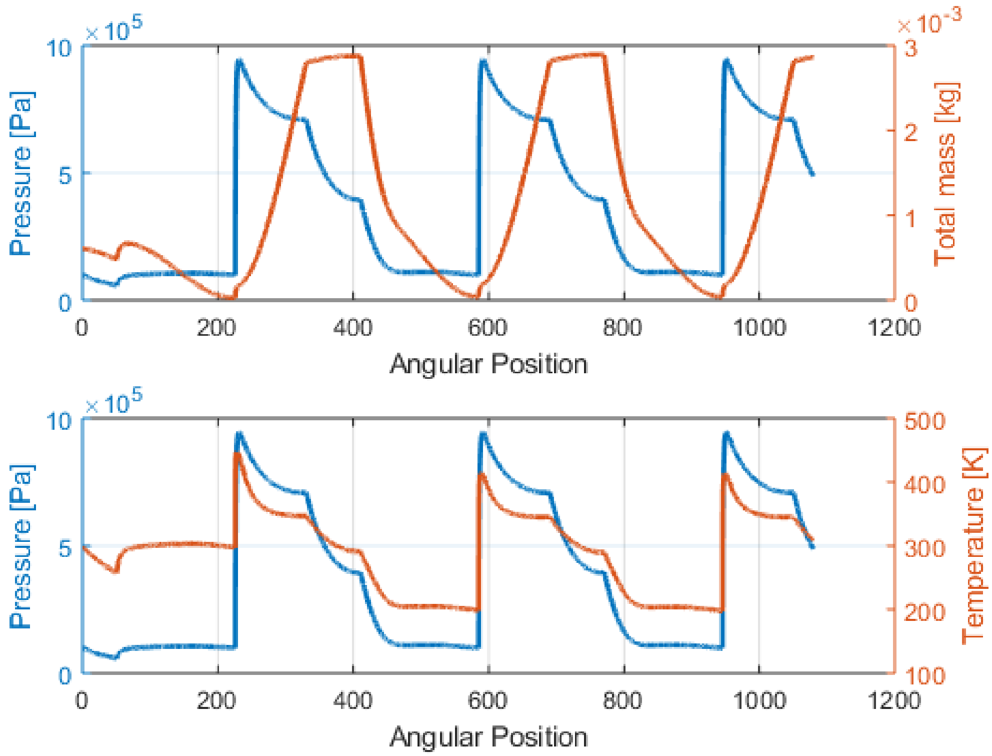

Figure 15: Comparison of Pressure vs Mass and Temperature of Control Volume 1

A consistent pattern emerges in each CV for pressure, temperature, and mass after the first transient (or equalizing) revolution. A single revolution is a very short amount of time for the whole system to reach equilibrium, however, this only occurs because this model currently assumes a constant RPM. This means that the losses and variation expected from a typical start-up of any engine are not truly represented as it was not a focus of this model. That said, due to the low RPM requirements of RVE, the start-up time is still much faster than that of a turbine (see Table 1).

Using control volume 1 (CV1) as an example (shown in Figure 15), the pattern repetition is consistent and in line with our expectation. Starting with the Pressure line, we see that all four CVs start at the same pressure and begins its cyclic shape once it has been fully exposed to the inlet port, which is located in-between $315°$ and $330°$. However, closer analysis shows that CV1 appears to encounter the inlet port at $225°$. This is because the angular rotation is read from the vane that represents the boundary at the back of the CV (noted as Vane 1). Meanwhile, the vane that is at the front of the CV (noted as Vane 2) is actually $90°$ ahead of Vane 1. Therefore, Vane 2 crosses the threshold for the inlet port at $315°$, which is when Vane 1 is at $225°$. That is why $225°$ marks the large spike in pressure.

After the spike in pressure due to the CV's initial exposure to the inlet port, it then appears to have three steps or three different slopes at during which the pressure decreases. The first more gradual decrease occurs due to two unfavorable circumstances: 1. The continued expansion of the CV during filling. 2. The decreased flow into the CV due to pressure normalization. These two factors combine to limit our model's ability to reach and maintain the set inlet pressure at the port of 1 MPa. The total mass curve validates this assessment as we see the mass continuously rise while the pressure and temperature dip slightly due to the continued expansion during the filling process and the reducing flow rate as stated in section 3.3 .

The next more pronounced decrease in pressure occurs as the inlet port and outlet port are closed off from the CV and only the leakage modeled through the end caps is present. The lowering pressure means that fluid from the adjacent chamber (which is exposed to the inlet port), would leak into the current CV. The leakage is represented by the slight increase in mass between $330°$ and $410°$ (or $50°$ for Vane 1 and

$140°$ for Vane 2); the region of closed ports. The reduced flow rate in, means a steeper drop in pressure while the expansion process continues. However, from section 3.4 Volume Integration in Polar Coordinates and Figure 10, we know that the maximum volume is at 410° which is why the outlet port is set to open at this point. If you do not begin exhausting the expanded fluid, you will begin to compress it, therefore, wasting energy. This also explains why the pressure curve appears to level out to a slop of 0 before the third and most drastic drop.

The final drop in pressure in a single revolution is due to the exhaustion of the expanded fluid out to the outlet port. This port is also subject to varying mass flow rate out and therefore, the pressure gradually normalizes to the ambient pressure. All while the volume of the CV continues to decrease to almost (but not exactly) zero. This is why the mass also approaches zero but never quite reaches it. This cycle begins again once Vane 2 is exposed to the inlet port.

Figure 16 and Figure 17, depict the changes to this cycle due to changes in the operating parameters. Figure 16 specifically shows what happens if you increase the mass flow rate by 400% (5 times the original m_{flow}). We see that the model is able to maintain higher pressures during the filling process, thereby vastly reducing the first dip seen in pressure on Figure 15. Additionally, because the inlet port closes at a high pressure, the subsequent drops in pressure are greater. Meanwhile, Figure 17 varies that the cycle is repeated consistently. Here, there fluid fluctuations are shown over 9 cycles, three times more than the original iteration. This shows that we can conserve memory and computational power by running at the original total of three revolutions and still get an accurate average value.

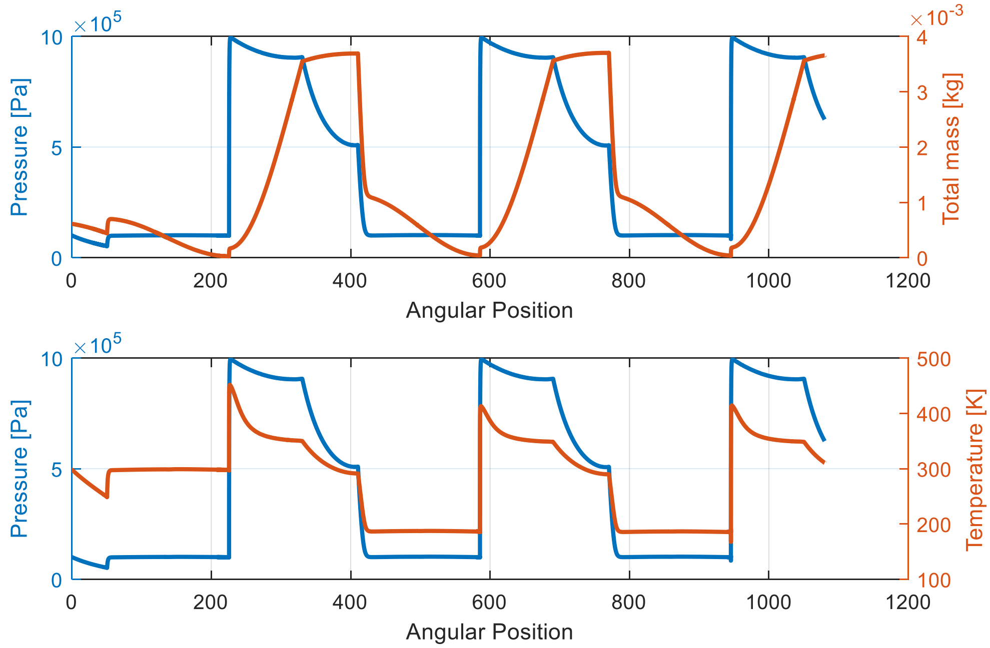

Figure 16: Comparison of Pressure vs Mass and Temperature of Control Volume 1 with Fives Times the Mass Flow Rate (m_{flow}= 0.75kg/s)

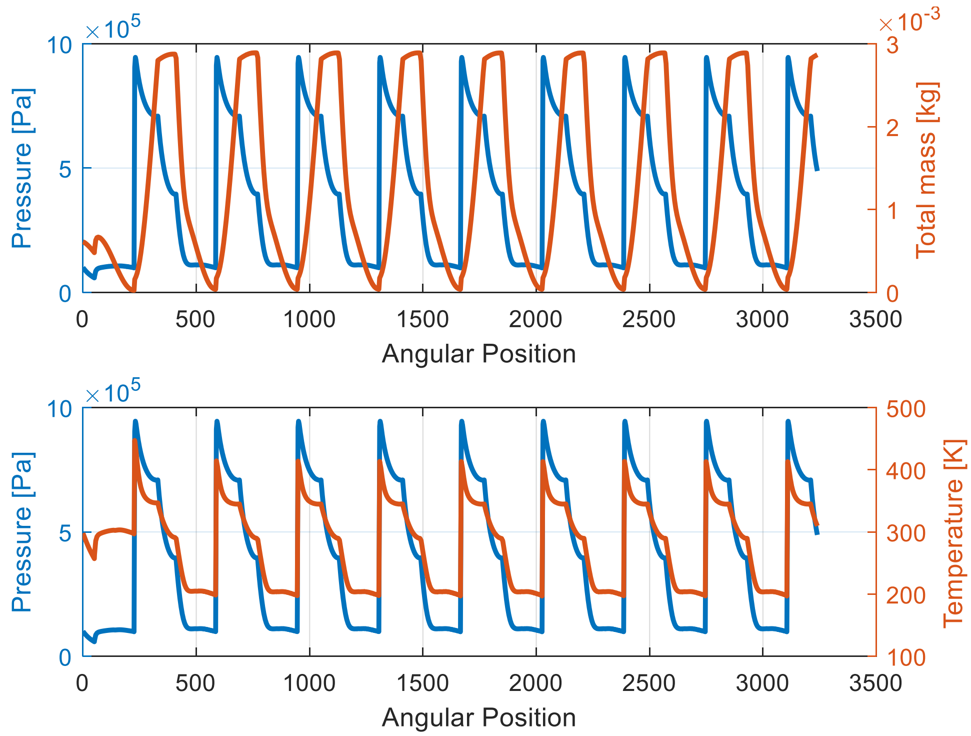

Figure 17: Comparison of Pressure vs Mass and Temperature of Control Volume 1 over an Extended Operation (9 Complete Cycles)

As mentioned earlier, all the results were computed while accounting for mass leakage between chambers. Figure 18, shows the mass changes in mass for a single CV due to leakage only. It clearly depicts the cyclic nature of the process; after about 180°, the pattern emerges. These fluctuations account for the fluids leaking in and out of the CV from the sides of the two adjacent vanes.

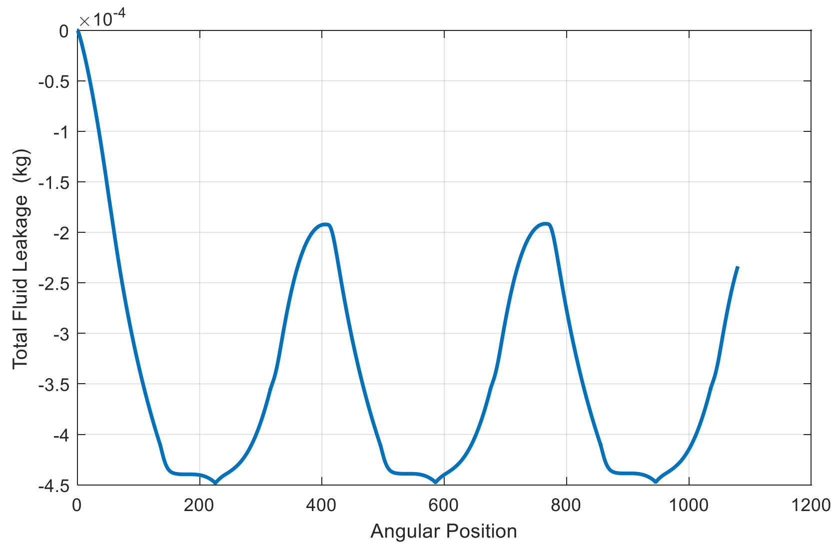

Figure 18: Changes in the Total Mass of Control Volume 1 Due to Leakage

4.3 Torque Impact on Single Vane and its Implications on RVE Dynamics

Using the results of pressure in a given working chamber and by performing force balances on each vane, our simulation can yield the torque on a single vane and the rotor. Both the moment arm for the force and the vane surface area on which pressure acts vary during rotation. RVEs use this variation in force and moment arm to optimize torque output by having the largest moment arm and vane surface area only in the high-pressure expansion zone, yielding positive torques.

Figure 19 depicts this efficient use of the eccentric RVE shape, as the cyclic process is essentially shifted up with the maximum torque on a single vane reaching 150 N-m and only dropping to approximately -25N-m of torque. Figure 20 transposes the net torque on Vane 1 (from Figure 19) onto a pressure plot of the pressure in the chambers ahead and behind that vane. The plot helps highlight the pressure fluctuations, as we clearly see that for a majority of the cycle the pressure behind the vane is greater than pressure ahead. This was to be expected, but the graph clearly shows you the magnitude of pressure difference during the segment in which the pressure ahead in greater. The negative torque zone is minimized by the reduced the moment arm and the peak of 0N-m represents a fully retracted vane; thus, no surface area for pressure.

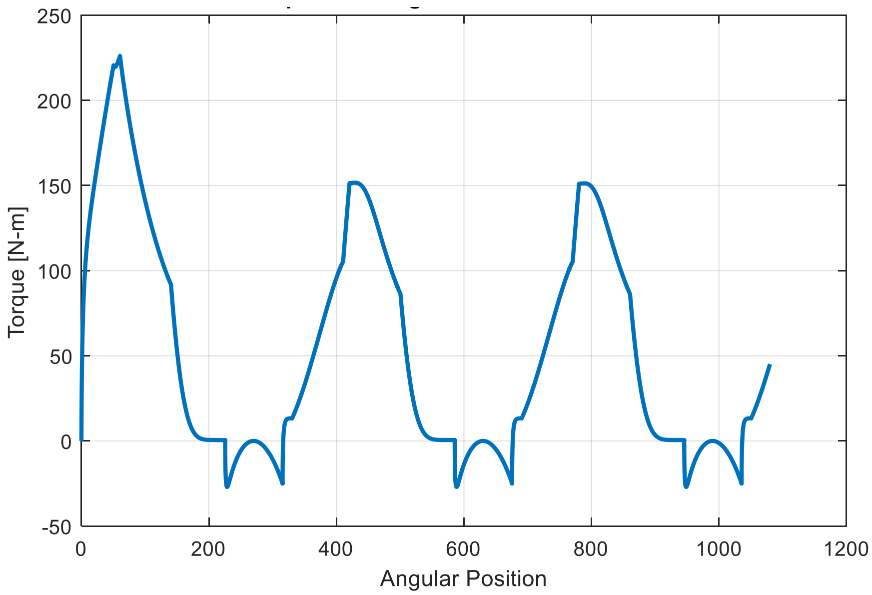

Figure 19: Plot of the Torque of a Single Vane Due to Pressure Difference

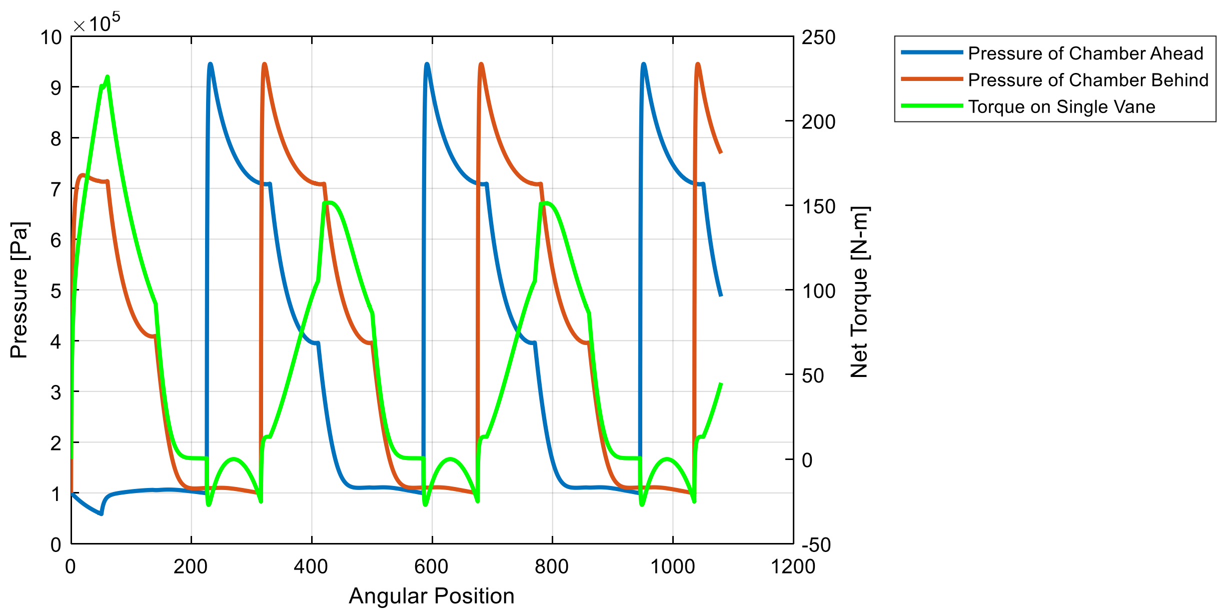

Figure 20: Comparison of Pressure Changes on Both Sides of the First Vane, Illustrating how the Difference Relates to Torque

By summing the torques on each vane, we can see that the negative torque has little impact on the net torque on the RVE rotor (shown in Figure 21). Each vane is only briefly subjected to negative torque, and during that phase, the other vanes are generating positive torque to compensate. The result is a more consistent average net torque of 184.7 N-m for all the vanes combined compared to an average torque of 52.7 N-m with higher fluctuations. Although there are some fluctuations in the net torque for all the vanes, the RVE spins at high enough RPM to further minimize the fluctuations being transmitted to craft or electrical generator. Therefore, we chose to use the average net torque in our further analysis of the RVE operations.

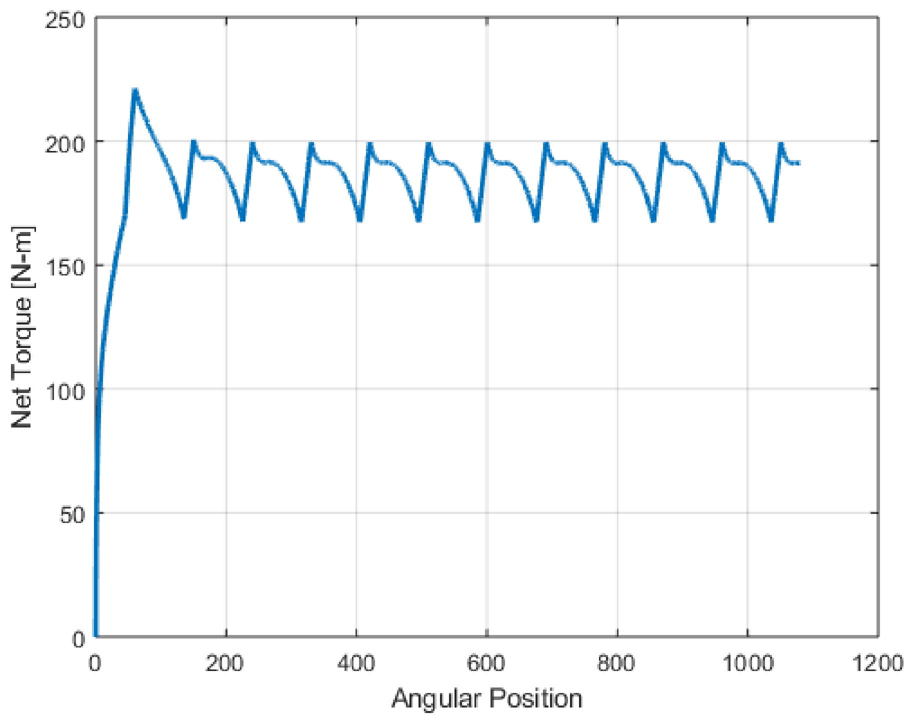

Figure 21: Plot of the Net Torque from All Vanes due to Pressure Difference

4.4 Mapping Power and Torque Performances Over Varying Operating Conditions:

The second program (basic_model_varying.m) adapts the first program (basic_model_single.m) to enable parametric studies. This allows us to generate performance plots over a wide range of conditions which is necessary to understanding the capabilities and limitations of an expander.

At present, the basic_model_varying.m model supports studies over varying mass flow-rates, rpm and inlet pressures. However, it is not limited to those and the script is dynamic and adjustable enough to generate plots for variations in other parameters like inlet and outlet temperature, fluid type (as long as ideal gas assumption applies) and the size of the RVE. We utilized this script to generate two charts commonly seen in a motor specification sheet; torque versus RPM (see Figure 22) and power versus torque (see Figure 23). Both yielded familiar trends, with peak torque occurring at the lowest RPM and the maximum power curve tapering off at lower torques.

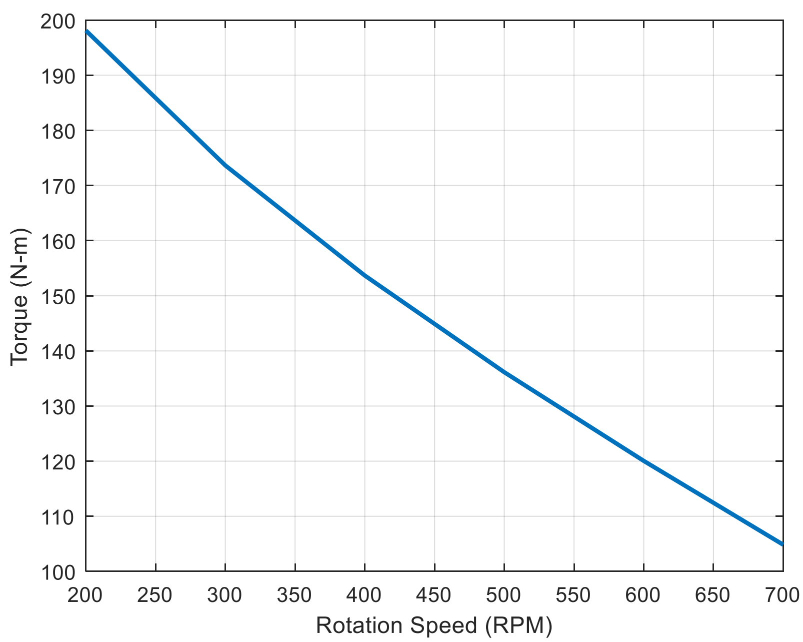

Figure 22: Plot of RPM and Torque at 100kpa and Mass Flow Rate of 0.15kg/s

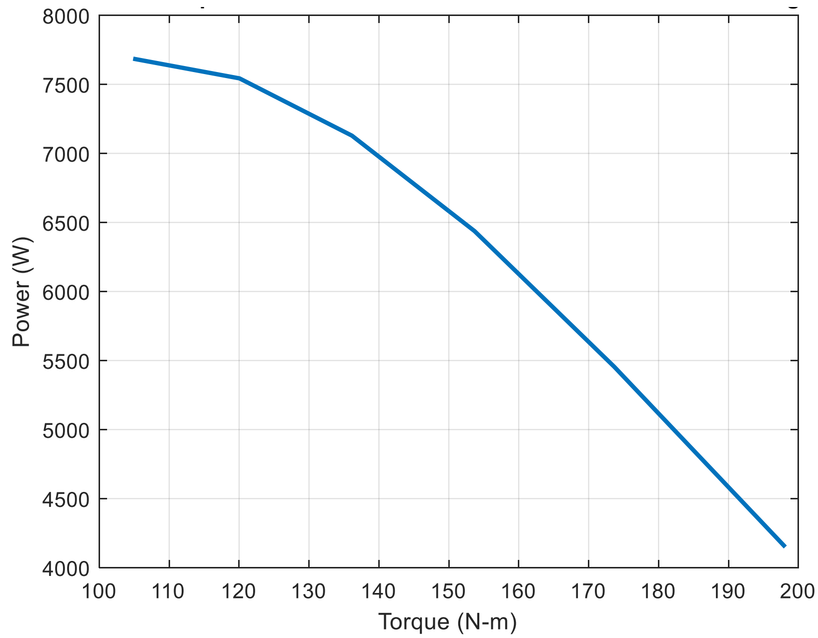

Figure 23: Plot of Torque vs. Power at 100kPa and Mass Flow Rate of 0.15kg/s

Additionally, we were also able to simulate performance over 15 various mass flow rates ranging from 0.01 to 0.50 kg/s and 6 different RPM ranging from 200 to 700 rpm, for a total of 90 different iterations. The results of output power for our 90 iterations simulation was then depicted by the use of surface and contour plots shown below (Figure 24 and Figure 25 respectively). The plots present the same data but in two different means to aid with the visualization of the results.

Figure 24 shows that the peak power occurs at highest RPM and mass flow rate, which is to be expected. It also suggests that at lower mass flow rates, higher RPMs can lead to worse power outputs. Figure 25 utilizes contour lines to mark out the region of negative power. For any given mass flow rate above 0.1kg/s, we see that increasing RPM can increase power more significantly at higher flow rates such as 0.3kg/s. Meanwhile, at 0.05kg/s flow rate, we see that speeds greater than 450rpm begin decreasing power. Power drops below the 2000W level at 550rpm and drops into the negative at 650rpm. This means that, at such high RPM and low flow rate, our system is working as a compressor and external energy would be needed to power the RVE.

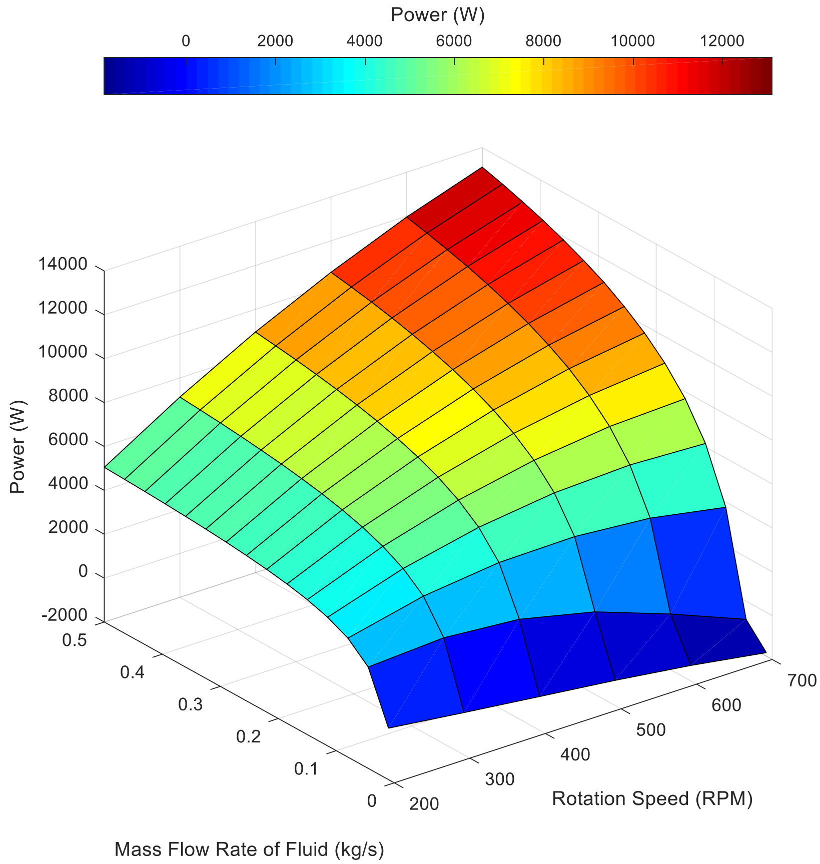

Figure 24: Surface Plot of RPM and Mass Flow Rate vs. Power at 100kPa

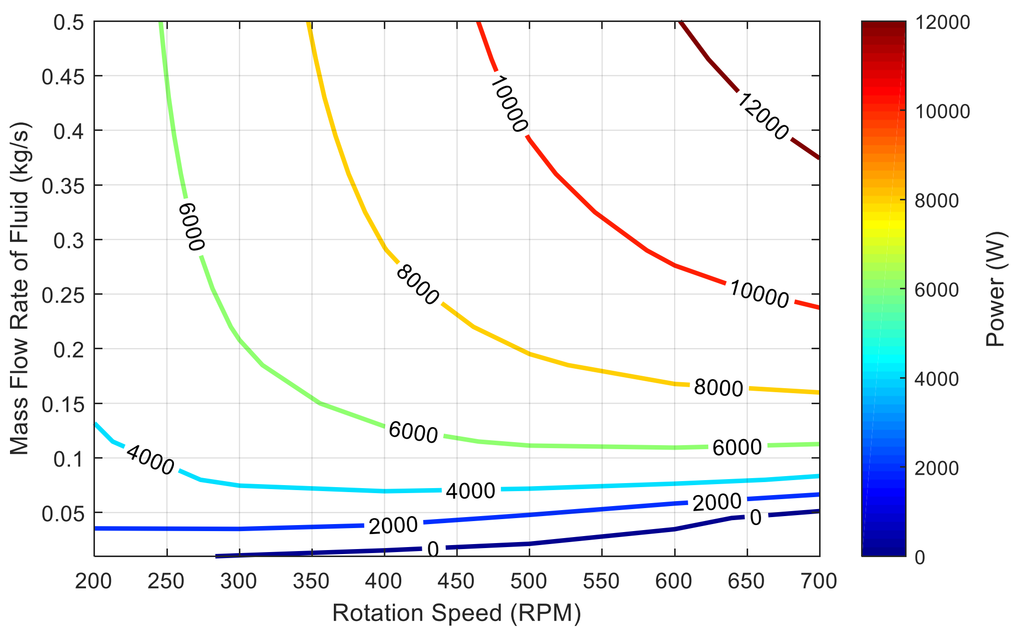

Figure 25: Contour Plot of RPM and Mass Flow Rate vs. Power at 100kPa

4.5 Mapping Efficiency Performances Over Varying Operating Conditions:

Using our second program, we were able to map out the efficiencies of the RVE over varying conditions similar to that of our power plots. Figure 26, depicts the efficiencies of the studied RVE onto a contour plot. It highlights two potential peaks; a low and high rpm peak. The high rpm peak appears to be operating close to a steep drop-off in efficiency, as a series of contour level are collected right next to it. This steep drop-off is verified by our surface plot and color map of the same efficiencies (see Figure 27 and Figure 28). In the surface plot and color map, we set a cut-off efficiency at "-10%", which is why they appear to be cropped. That illustrates the significance of knowing the location of our performance drop-off. These figures also show us that the lower rpm peak is the most efficient, as is approached 27.77% efficiency. However, the low rpm peak is similarly close to a drop-off. This suggests that during the designing phase, we should not aim for the peaks but regions of more consistent efficiencies.

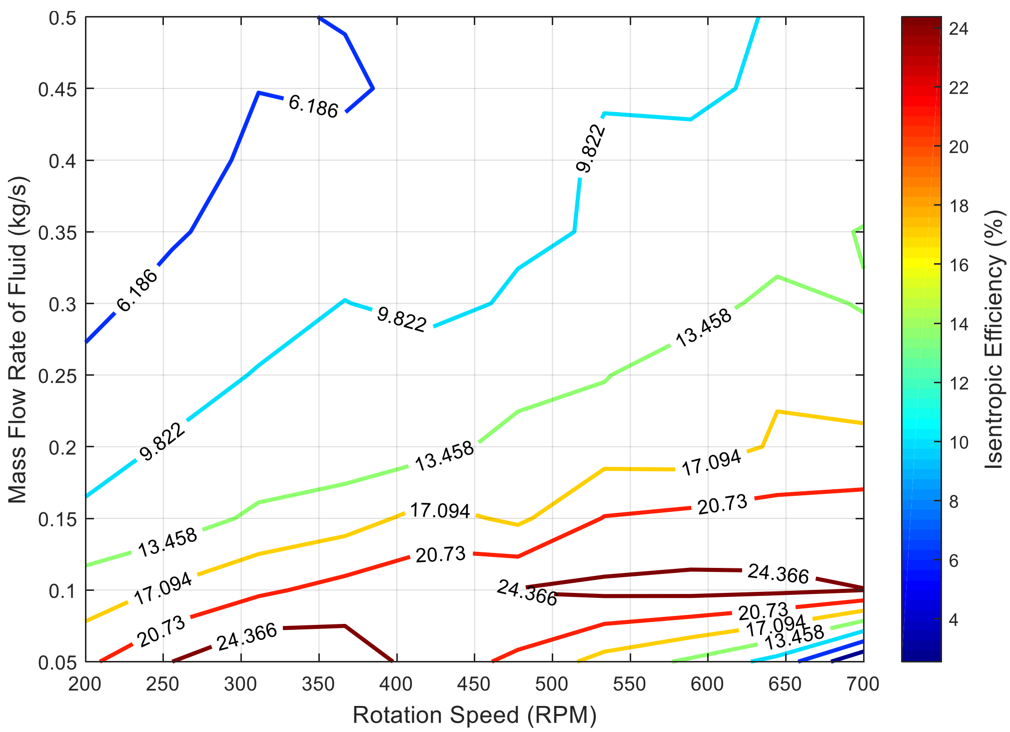

Figure 26: Contour Plot of RPM and Mass Flow Rate vs. Isentropic Efficiency

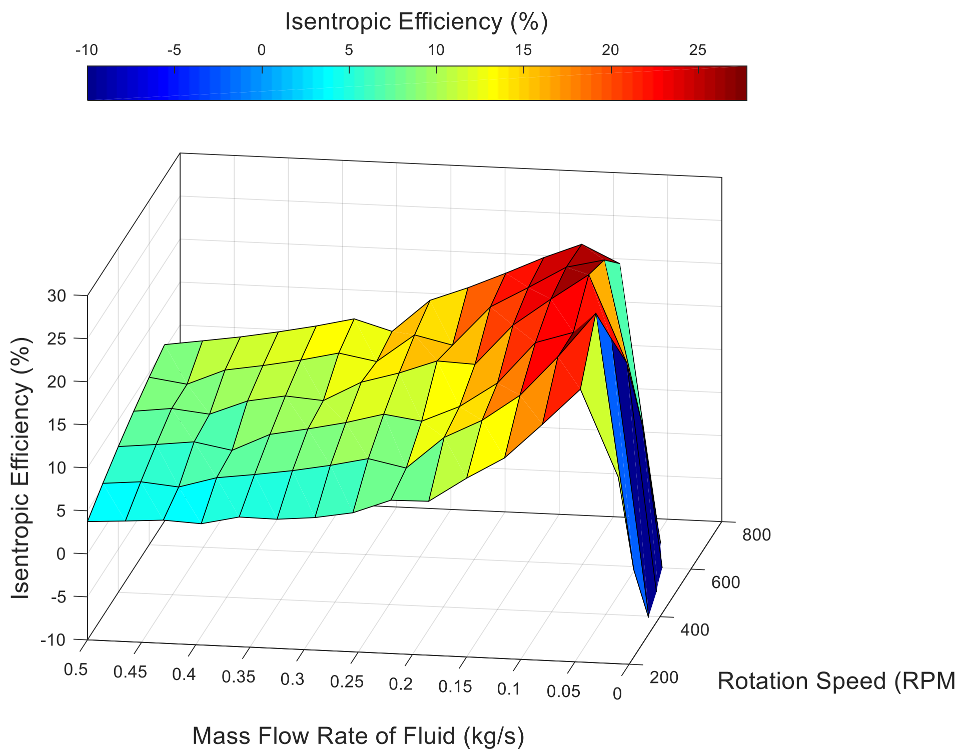

Figure 27: Surface Plot of RPM and Mass Flow Rate vs. Isentropic Efficiency

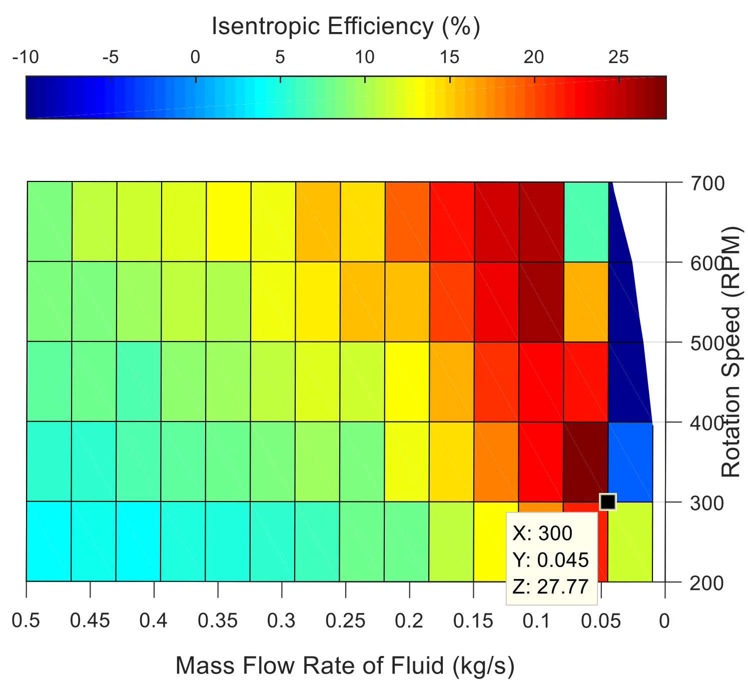

Figure 28: Color Map of RPM and Mass Flow Rate vs. Isentropic Efficiency

A final plot presents efficiency tradeoffs between power and torque at a fixed mass flow rate. The second script was used to generate Figure 29 at 1MPa inlet pressure, a fixed mass flow rate of 0.15kg/s and varying rpm. We see that power increases with efficiency because we can generate more power at higher rotational speeds. Whereas, torque decreases with increasing efficiency because as Figure 22 shows, we generate the most torque at the lowest rotational speed. The colormap (Figure 28), helps with illustrating the relationship between efficiency and rpm at a fixed mass flow rate. With the exception of operations at slower mass flow rates, we see that efficiency increased with rpm at a fixed mass flow rate.

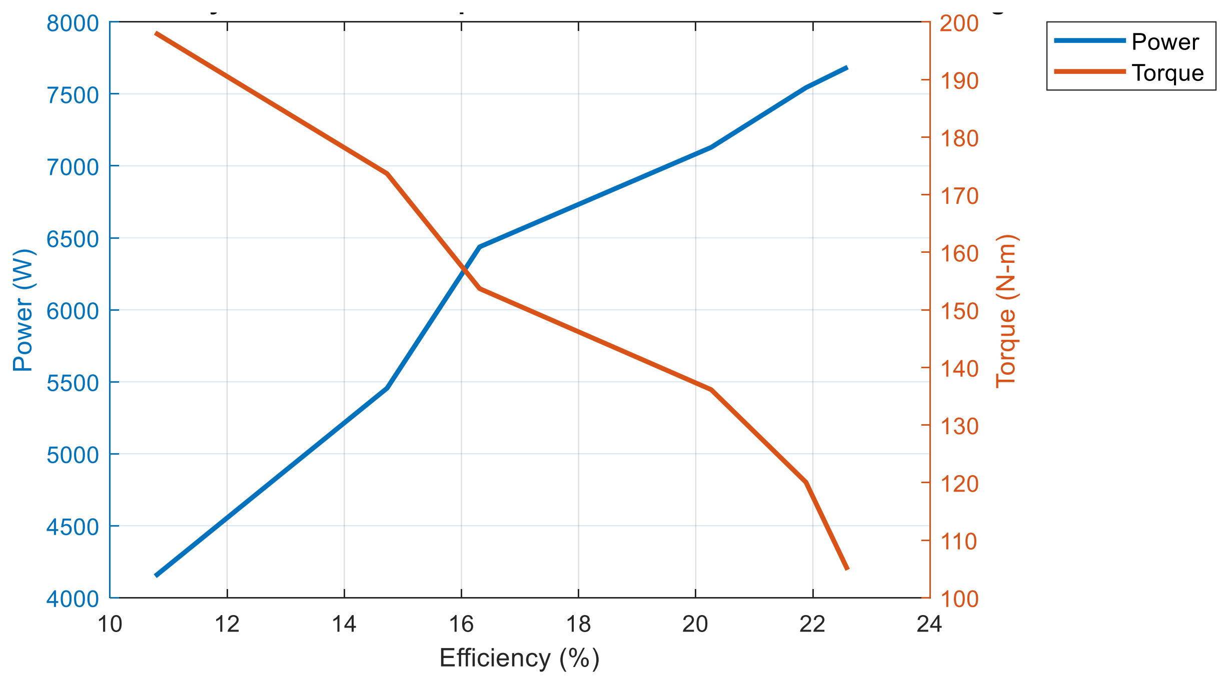

Figure 29: Plot of Power and Torque vs. Efficiency at Mass Flow Rate of 0.15kg/s

The low isentropic efficiencies are an inherent nature of RVE due to their geometric simplicity compared with turbine expanders with hundreds of aerodynamically shaped vanes designed to extract as much energy as possible from a high enthalpy fluid. This means that it is hard to extract the maximum energy possible from the working fluid. However, this is less of an issue compared to the extreme RPM requirements of turbine expanders when operating in small capacities.

Chapter 5

Concluding Remarks:

Tasked with developing a power system that could enable an extended Landed Venus mission, this study focused on creating a dynamic model capable of predicting engine performances for the selected rotary vane expander. The results generated by the code shows that this thesis has laid the necessary groundwork to for the development, building, and testing of future experimental and numerical assessment of a rotary vane expander working with exotic working fluids. Through detailed analysis of prior studies and application of thermo-fluid dynamics, the resultant model is capable of predicting the pressures, mass, and temperature in each CV. With this, we were able to generate an estimate of the net power, net torque, and efficiencies over a wide array of operating conditions.

By applying assumptions validated in prior studies, we were also able to estimate some of the losses, such as frictional and mass losses, a typical RVE might experience. However, we are still in the process of building a physical test plant to validate this model. Ideally, an off-the-shelf RVE unit would need to be purchased and operated under various conditions to determine our model's accuracy. The unit might need to be disassembled to gather all the necessary information the code requires such as inlet and outlet port location and other dimensioning.

Some of the currently know limitations of this model that will be improved upon during future updates are the filling and evacuating modeling of a CV. We know that there should be a defined relationship for the rate at which fluid enters and leaves a CV that is a function of the variation in pressures in the CV and of the fluid source/sink. Additionally, most RVE have their rotation speeds controlled by their mass flow rate, this model does not currently have a set relationship between those two variables and they are treated as independent operating conditions.

Not all leakage paths were modeled as we were able to make some assumption that may not necessarily apply to all RVE designs, such as the seals between the inlet and outlet port. We also assumed perfect contact between the vanes and the stator, but a full vane dynamic model must be performed, similar to that done in G. Bianchi and R. Cipollone [11]. J. Xiaohan *et al*. [4] study showed that even with springs there might occasional losses of contact, although they are greatly reduced. Lastly, fluidic assumptions such as ideal gas and constant specific heats (cp & cv), need to be addressed for each working fluid. Operating a non-ideal gas like vapor mercury would require functions to output all the necessary fluid properties (including density, pressure, etc.) at all condition

The two MATLAB programs will enable future development of a Venus power cycle. It generates estimates of power and torque that are necessary for an iterative design process of the entire power cycle. Those estimates along with our isentropic efficiencies were comparable to that of other RVE systems. Future modifications of both scripts will be placed in an online repository and updated as need.

Appendix A

Individual CV Simulation

```
% basic_model_single.m
% Programmer:          Tamuno-Negiyeofori B Warmate
% Thesis Supervisor:   Alexander S Rattner
% Honors Advisor:      Daniel Cortes
% Schreyer Honors College Research Work
% Date:                04/08/18
% Description: This program models the operations of individual working chambers in a
% rotary vane expander. It produces intermediate plots of the thermodynamic properties (i.e. Mass,
% Temperature and Pressure), friction, leakage, torque, and power for each working chamber

clc; clear; close all;

%% Defining Variables
% Working Fluid's Operating Properties
P_H = 10e5; % [Pa] proposed inlet pressure
P_L = 1e5; % [Pa] proposed outlet pressure
T_H = 350; % [K] proposed inlet temperature
T_L = 298; % [K] proposed outlet temperature
m_flow = 0.15; % [kg/s] mass flow rate into system
cp = 1.006e3; % [J/kg-K] for air
cv = 0.73e3; % [J/kg-K] for air
k  = cp/cv; % Ratio of specific heats
Rs = cp-cv;

% RVE Geometric Dimensions and Simulation Port Locations
R = 0.1; % [m] radius of large cylinder
e = 0.2*R; % [m] eccentric distance
z = 0.1; % [m] depth/length of rotor
Vanes = 4; %number of vanes
% Note: CCW is positive, so inport on the right and outport is on the left
in_port = deg2rad(wrapTo360(315:330)); % [rad] inlet port angle range
out_port = deg2rad(140:225); % [rad] outlet port angle range
n_rev = 4; % total number of revolutions
rpm = 300; % [rev/min]
omega = rpm*(2*pi/60); % [rads/s]
sim =[0,2*pi+2*pi*n_rev]; % simulation space


%% Establishing Control Volume
% Forming geometry
d_theta = 0:deg2rad(1):2*pi; % going CCW
```

```
% initialization
RR = zeros(1,length(d_theta));
for ii = 1:length(d_theta)
    RR(ii) = cal_L(e,R,d_theta(ii));
end

% Checking the radius of the rotor (rr)
rr(1,1:length(d_theta)) = mean([cal_L(e,R,3*pi/2),cal_L(e,R,pi/2)])-e;


% Integration in polar coordinates
% Defining function for upper bound of radial integration
upperBound = @(theta) sqrt(e^2+R^2-(2*e*R*cos(pi/2+theta-asin(cos(theta)*e/R))));
% Looping to find CV at theta of every 1/2 degrees
d_angle = deg2rad(0.5); % [rad] loop step angle
angles = sim(1):d_angle:sim(2); % [rad] range of stepped angles
d_vane = 2*pi/Vanes; % [rad] angle between vanes
V = zeros(1,length(angles));
% Performing integration for each angle and its storing volume
for ii = 1:length(angles)
    CV_ang = [angles(ii), angles(ii)+d_vane]; % integration bounds
    V(ii) = abs(integral2(@(theta, r) r, CV_ang(1),CV_ang(2), rr(1), upperBound)) *z;
end

%% Fitting Volume to a sine function for ODE
V_time = angles/omega;
[pks, locs] = findpeaks(V,V_time);
amp = (max(V)-min(V))/2;
freq = 2*pi/mean(diff(locs));
shift = min(V)+amp;
phase = omega*wrapTo2Pi(locs(end))-(pi/2);
simV = amp*sin(freq*V_time-phase)+shift;

% compare dvdt
test_dVdt = diff(V)./diff(V_time);
fit_dVdt = amp*freq*cos(freq*V_time-phase);
% error calculation
V_error = mean(abs((V-simV)./V));
dVdt_error = mean(abs((test_dVdt-fit_dVdt(1:end-1))./test_dVdt));

% Storing coefficients for use in derivative
trig_C = [amp;freq;phase;shift];

%% ODE45 Modelling
% ode conditions
max_step = 1.5e-4;
tspan = [V_time(1), V_time(end)-(2*pi/omega)];
options = odeset('MaxStep', max_step);
```

```
% setting time for each chamber (CV_t)
t_vane = d_vane/omega;
CV_t(1:Vanes,1) = linspace(V_time(1),V_time(1)+t_vane*(Vanes-1),Vanes);

% defining initial conditions
V_int = amp*sin(freq.*CV_t-phase)+shift; % Inital Volume
T_int(1:Vanes,1) = T_L; % Inital Temp.
M_int = (P_L./(Rs.*T_int)).*V_int; % Inital Mass
L_int = zeros(4,1); % Inital Leakage
initial_C = [M_int;T_int;V_int;L_int]; % All intial conditions

% Other Constants for ODE
Port_C = [P_H, P_L,T_H, T_L];
R_interp = [d_theta;RR;rr]';

% Calling the ode45 function
% Note: M_T stores all thermodynamic properties and outputs of ode45
% Order is Mass,Temp,Volume, and Total Leakage; For all CVs
tic
[t, M_T] = ode45(@(t,M_T)
odefun(t,M_T,d_vane,m_flow,Rs,cp,cv,Port_C,trig_C,R_interp,omega,Vanes,in_port,out_port),...
    tspan,initial_C,options);
toc

%% Plotting Pressure versus Mass and Temperature angle for each CV
for mm = 1:Vanes
    % Using time value from ode for all calculations and position estimate
    theta(:,mm) = t*omega+(mm-1)*d_vane;
    % Getting all Volume changes for specifc CV
    V_m(:,mm) = M_T(:,Vanes*2+mm);
    % Using Ideal gas law to solve for Pressure at every moment in time
    P_ms(:,mm) = (M_T(:,mm).*M_T(:,Vanes+mm)*Rs)./V_m(:,mm);

    figure()
    % Pressure and Mass subplot
    subplot(2,1,1)
    % double y axis plot of pressure and mass
    yyaxis left
    plot(rad2deg(theta(:,mm)),P_ms(:,mm),'LineWidth',2)
    title(['Comparison of Pressure versus Mass and Temperature of Control Volume ',num2str(mm)])
    ylabel('Pressure [Pa]')
    xlabel('Angular Position')

    yyaxis right
    plot(rad2deg(theta(:,mm)),M_T(:,mm),'LineWidth',2)
    ylabel('Total mass [kg]')
    grid on
```

```
 % Pressure and Temperature subplots
  subplot(2,1,2)
  yyaxis left
  plot(rad2deg(theta(:,mm)),P_ms(:,mm),'LineWidth',2)
  ylabel('Pressure [Pa]')
  xlabel('Angular Position')

  yyaxis right
  plot(rad2deg(theta(:,mm)),M_T(:,Vanes+mm),'LineWidth',2)
  ylabel('Temperature [K]')
  grid on

end

%% Torque calculations
% Calculating tangential distance for each vane. i.e. moment arm of pressure force
tan_r = (cal_L(e,R,theta)+rr(1))/2;
% Calculating the total area, the pressure can act on each vane
tan_area = (cal_L(e,R,theta)-rr(1))*z;

torque = zeros(length(theta(:,1)),Vanes);
net_torque = zeros(1,length(theta(:,1)));
for ii = 1:length(theta(:,1))
  % Note: CCW is positive
  % Need to determine what pressures are acting on each vane
  for jj = 1:Vanes
    % defining the Pressure from Adjacent CV
    if jj == 1
      adj = Vanes;
    else
      adj = jj-1;
    end
    % individual torque calculations
    torque(ii,jj) = (P_ms(ii,adj)-P_ms(ii,jj)).*tan_area(ii,jj).*tan_r(ii,jj);
  end
  net_torque(ii) = sum(torque(ii,:)); % Total net torque at each moment in time
end

% Net torque plot
figure()
plot(rad2deg(theta(:,1)),net_torque,'linewidth', 2)
title('Plot of the Net Torque from All Vanes due to Pressure Difference')
xlabel('Angular Position')
ylabel('Net Torque [N-m]')
grid on
```

```
50
% Individual torque plot
figure()
plot(rad2deg(theta(:,1)),torque(:,1), 'linewidth', 2)
title('Plot of the Torque of a Single Vane due to Pressure Difference')
xlabel('Angular Position')
ylabel('Net Torque [N-m]')
grid on

% Torque to Pressure comparison
figure()
yyaxis left
plot(rad2deg(theta(:,1)),P_ms(:,1),rad2deg(theta(:,1)),P_ms(:,4), 'linewidth', 2)
title('Comparison of Pressure Changes on Both Sides of Vane 1')
ylabel('Pressure [Pa]')
yyaxis right
plot(rad2deg(theta(:,1)),M_T(:,Vanes*3+1))
xlabel('Angular Position')
grid on
legend('Pressure of Chamber Ahead','Pressure of Chamber Behind','Location','northeastoutside')

%% Friction modeling
% Centrifugal and spring forces only

% Defining constants for individual vane
spring_k = 5000; %[N/m] about 30lb/in
spring_l = 0.0675; %[m] spring free height
min_l = 0.025; %[m] length at max. compression
vane_l = rr(1)-min_l; %[m] length of the vane
vane_w = rr(1)*1/8; %[m] width of vane approximated
coef_f = 0.2; % coefficient of friction
rho_vane = 8000; %[kg/m^3] density if ss316 to find mass of
mass_vane = rho_vane*z*vane_l*vane_w;

% Alert user if spring is not long enough to maintain a force on it during
% maximum extension
if vane_l+spring_l < max(RR)
    error('Spring is not long enough to maintain vane contact with stator')
end

% Calculating friction values at each individual vane
compression_l = (vane_l+spring_l) - cal_L(e,R,theta); %[m] length the spring is compressed
f_spring = compression_l * spring_k; %[N] Spring force
% Centrifugal force below
f_centr = mass_vane.*(omega.*(cal_L(e,R,theta)-vane_l/2)).^2./(cal_L(e,R,theta)-vane_l/2); %[N]
f_fric =  (f_spring+f_centr)* coef_f; %[N] Frictional force
t_fric = f_fric.*cal_L(e,R,theta); %[N-m] Frictional torque lost
p_fric = f_fric.*omega.*cal_L(e,R,theta); %[W] Frictional power lost
```

```
% Net values of friction
netF_fric = sum(f_fric,2); %[N] total net friction at every point in cycle
netT_fric = sum(t_fric,2); %[N-m]
netP_fric = sum(p_fric,2); %[W]

% Plot Net Frictional Torque from All Vanes
figure()
plot(rad2deg(theta(:,1)),netT_fric,'linewidth', 2)
title('Plot of the Net Frictional Torque from All Vanes')
xlabel('Angular Position')
ylabel('Net Frictional Torque [N-m]')
grid on

% Compare normal forces (Spring vs. Centrifugal)
figure()
plot(rad2deg(theta(:,1)),f_spring(:,1),rad2deg(theta(:,1)),f_centr(:,1),'linewidth', 2)
title('Plot of the Spring and Inertial Centrifugal Normal Forces')
xlabel('Angular Position')
ylabel('Force [N]')
legend('Spring','Inertial Centrifugal')
grid on

% Plot Individual Friction on a Vane
figure()
plot(rad2deg(theta(:,1)),t_fric(:,1), 'linewidth', 2)
title('Plot of the Frictional Torque on a Single Vane')
xlabel('Angular Position')
ylabel('Net Torque [N-m]')
grid on

% Plot Net Friction Power Lost from All Vanes
figure()
plot(rad2deg(theta(:,1)),netP_fric,'linewidth', 2)
title('Plot of the Net Friction Power of All Vanes')
xlabel('Angular Position')
ylabel('Net Frictional Torque [W]')
grid on


%% ODE Function
function y =
odefun(t,M_T,d_vane,m_flow,Rs,cp,cv,Port_C,Trig_C,R_interp,omega,Vanes,in_port,out_port)
% defining position based on time
theta = t*omega;
% setting time and position for each chamber
CV_p(1:Vanes,1) = linspace(theta,theta+d_vane*(Vanes-1),Vanes);%Control V. position
CV_t = CV_p/omega; %Control V. position
```

```
% estimate for dV/dt
amp = Trig_C(1); freq = Trig_C(2); phase = Trig_C(3);
dVdt = amp*freq*cos(freq.*CV_t-phase);

% setting up location checks
Loc = zeros(Vanes,90);
for ll = 1:Vanes-1
   Loc(ll,:) = wrapTo2Pi(CV_p(ll):deg2rad(1):CV_p(ll+1)-deg2rad(1));
end
Loc(Vanes,:) = wrapTo2Pi(CV_p(end):deg2rad(1):CV_p(end)+d_vane-deg2rad(1));
Loc = round(rad2deg(Loc));

% Pressure calculations
P_H = Port_C(1); P_L = Port_C(2); T_H = Port_C(3); T_L = Port_C(4);
% Using Ideal gas: P = m*R*T/V
P_ms = (M_T(1:Vanes).*Rs.*M_T(Vanes+1:Vanes*2))./M_T(Vanes*2+1:Vanes*3);

%Leakage calculation
% Radius for leakage integration
RR = interp1(R_interp(:,1),R_interp(:,2),wrapTo2Pi(CV_p),'spline');
mu = 25e-6; %dynamic viscosity approx. for air at 450K, P not relevant
vane_w = R_interp(1,3)*1/8; %[m] width of vane approximated
rho_a = 0.785; % average density estimate
dP_dx = [P_ms(end)-P_ms(1);-diff(P_ms)]/vane_w; %P1-P2 for pressure drop, so -diff needed
gap = 0.1e-3; %[m] estimated gap on both sides
% BCs and Integration Constant: u(y=0) = 0 and u(y=gap) = U = omega*r
% c2 = 0
% c1 = (U - (gap^2*dP_dx/(2*mu)))/gap;

% initialization
dmdt = zeros(Vanes,1);
dTdt = zeros(Vanes,1);
m_leak = zeros(Vanes,2);
for mm = 1:Vanes
   % Leakage integration needed in for loop
   % NSvelocity1 is for the 1st vane boundary of CV
   m_leak(mm,1) = (rho_a*gap*(RR(mm)-R_interp(mm,3))*(3*mu*omega*(RR(mm)+R_interp(mm,3))
...
      - dP_dx(mm)*gap^2))/(12*mu);

   % NSvelocity2 is for the front/next vane boundary of CV
   nn = mm + 1;
   if nn == Vanes +1
      nn = 1;
   end
   m_leak(mm,2) = (rho_a*gap*(RR(nn)-R_interp(nn,3))*(3*mu*omega*(RR(nn)+R_interp(nn,3)) ...
      - dP_dx(nn)*gap^2))/(12*mu);
```

```
% determining what CV leaks in which direction for flow1
    if m_leak(mm,1) > 0 && mm > 1
        leak1 = mm -1;
    elseif m_leak(mm,1) > 0 && mm == 1
        leak1 = Vanes;
    elseif m_leak(mm,1) < 0
        leak1 = mm;
    else
        leak1 = NaN;
    end
    % determining what CV leaks in which direction for flow2
    if m_leak(mm,2) > 0
        leak2 = mm;
    elseif m_leak(mm,2) < 0 && mm == Vanes
        leak2 = 1;
    elseif m_leak(mm,2) < 0 && mm < Vanes
        leak2 = mm+1;
    else
        leak2 = NaN;
    end

    % Thermodynamics Calculations
    if any(ismember(Loc(mm,:),rad2deg(in_port))',1) %open inlet port
        inflow = m_flow*(P_H - P_ms(mm))/P_ms(mm);
        dmdt(mm,1) = inflow + m_leak(mm,1) - m_leak(mm,2);
        dTdt(mm,1) = (-P_ms(mm)*dVdt(mm) + cp*inflow*T_H + cp*m_leak(mm,1)*M_T(Vanes+leak1)
...
            - cp*m_leak(mm,2)*M_T(Vanes+leak2)-
cv*dmdt(mm)*M_T(Vanes+mm))*(1./(M_T(mm)*cv));
    elseif any(ismember(Loc(mm,:),rad2deg(out_port))',1) % open outlet port
       outflow = m_flow*(P_L - P_ms(mm))/P_ms(mm);
        dmdt(mm,1) = outflow + m_leak(mm,1) - m_leak(mm,2);
        dTdt(mm,1) = (-P_ms(mm)*dVdt(mm) + cp*outflow*M_T(Vanes+mm) +
cp*m_leak(mm,1)*M_T(Vanes+leak1) ...
            - cp*m_leak(mm,2)*M_T(Vanes+leak2)-
cv*dmdt(mm)*M_T(Vanes+mm))*(1./(M_T(mm)*cv));
    else %ports closed, only leakage
        dmdt(mm,1) = (m_leak(mm,1)-m_leak(mm,2));
        dTdt(mm,1) = (-P_ms(mm)*dVdt(mm)+ cp*m_leak(mm,1)*M_T(Vanes+leak1) ...
            - cp*m_leak(mm,2)*M_T(Vanes+leak2)-
cv*dmdt(mm)*M_T(Vanes+mm))*(1./(M_T(mm)*cv));
    end
end
y = [dmdt;dTdt;dVdt;m_leak(:,1)-m_leak(:,2)];
end

%% Dimensioning function
function L = cal_L(e,R,theta)
L = sqrt(e^2+R^2-(2*e*R.*cos(pi/2+theta-asin(cos(theta).*e/R))));
end
```

Appendix B

Performance and Efficiency Simulation

```
% basic_model_varying.m
% Programmer:          Tamuno-Negiyeofori B Warmate
% Thesis Supervisor:    Alexander S Rattner
% Honors Advisor:       Daniel Cortes
% Schreyer Honors College Research Work
% Date:                04/08/18
% Description: This program models the performance and efficiency of a rotary vane expander
% over an array of operating conditions. It maps the power, torque, and efficiency.
% Currently, rpm, mass flow rate and inlet pressure can be varied.

clc; clear; close all;

%% Defining array of variable operating conditions
P_H = linspace(10e5,100e5,2); % [Pa] proposed inlet pressure
m_flow = linspace(0.01,0.5,15); % [kg/s] mass flow rate into system
rpm = linspace(200,700,6); % [rev/min]

%% Running and Storing iterations
plotPower = zeros(length(P_H),length(m_flow),length(rpm));
plotTorque = zeros(length(P_H),length(m_flow),length(rpm));
plotEff = zeros(length(P_H),length(m_flow),length(rpm));
% Note: Only 1 pressure being run in this version
for simP = 1%:length(P_H)
    for simM = 1:length(m_flow)
        for simR = 1:length(rpm)
            P_T_E = simu(P_H(simP),m_flow(simM),rpm(simR));
            plotPower(simP,simM,simR) = P_T_E(1);
            plotTorque(simP,simM,simR) = P_T_E(2);
            plotEff(simP,simM,simR) = P_T_E(3);
        end
    end
end

%% Plotting Power results
% Specify regions to be plotted
pressure_plot = 1;
massf_plot = 5;
pPower_map(:,:) = plotPower(pressure_plot,:,:);
```

```
% Surface Power plot
figure()
surf(rpm,m_flow,pPower_map)
title(['Surface Plot of RPM and Mass Flow Rate vs. Power at ',num2str(P_H(pressure_plot)/10e3),'kPa'])
xlabel('Rotation Speed (RPM)')
ylabel('Mass Flow Rate of Fluid (kg/s)')
zlabel('Power (W)')
colormap('jet');
c = colorbar;
c.Label.String = 'Power (W)';

%Contour Power plot
figure()
contour(rpm,m_flow,pPower_map,'Linewidth',2)
title(['Contour Plot of RPM and Mass Flow Rate vs. Power at ',num2str(P_H(pressure_plot)/10e3),'kPa'])
xlabel('Rotation Speed (RPM)')
ylabel('Mass Flow Rate of Fluid (kg/s)')
zlabel('Power (W)')
colormap('jet');
c = colorbar;
c.Label.String = 'Power (W)';
grid on

%% Comparison of Torque, Power and Efficiency
% sorting arrays needed for comparison
pTorque(1,:) = plotTorque(pressure_plot,massf_plot,:);
pPower(1,:) = plotPower(pressure_plot,massf_plot,:);
pEffi(1,:) = plotEff(pressure_plot,massf_plot,:);

% RPM vs Torque
figure()
plot(rpm,pTorque,'Linewidth',2)
title(['Plot of RPM and Torque at ',num2str(P_H(pressure_plot)/10e3),'kPa and Mass Flow Rate of ',
num2str(m_flow(massf_plot)),'kg/s'])
xlabel('Rotation Speed (RPM)')
ylabel('Torque (N-m)')
grid on

% Power vs. Torque
figure()
plot(pTorque,pPower,'Linewidth',2)
title(['Plot of Torque vs Power at ',num2str(P_H(pressure_plot)/10e3),'kPa and Mass Flow Rate of ',
num2str(m_flow(massf_plot)),'kg/s'])
ylabel('Power (W)')
xlabel('Torque (N-m)')
grid on
```

```
% Efficiency vs Power and Torque
figure()
yyaxis left
plot(pEffi,pPower,'Linewidth',2) % at fixed mass but varying rpm
title(['Plot of Efficiency vs Power and Torque at ',num2str(P_H(pressure_plot)/10e3),'kPa and Mass Flow
Rate of ', num2str(m_flow(massf_plot)),'kg/s'])
ylabel('Power (W)')
xlabel('Efficiency (%)')
grid on
yyaxis right
plot(pEffi,pTorque,'Linewidth',2) % at fixed mass but varying rpm
ylabel('Torque (N-m)')
legend('Power','Torque')
%% Efficiency Mapping Only
% Contour Efficiency
figure()
pEff_map(:,:) = plotEff(pressure_plot,:,:);
contour(rpm,m_flow,pEff_map,8,'Linewidth',2)
title({['Contour Plot of RPM and Mass Flow Rate'],[' vs. Isentropic Efficiency at
',num2str(P_H(pressure_plot)/10e3),'kPa']})
xlabel('Rotation Speed (RPM)')
ylabel('Mass Flow Rate of Fluid (kg/s)')
colormap('jet');
c = colorbar;
c.Label.String = 'Isentropic Efficiency (%)';
grid on

% Surface Effieciency
figure()
surf(rpm,m_flow,pEff_map)
title({['Surface Plot of RPM and Mass Flow Rate'],[' vs. Isentropic Efficiency at
',num2str(P_H(pressure_plot)/10e3),'kPa']})
xlabel('Rotation Speed (RPM)')
ylabel('Mass Flow Rate of Fluid (kg/s)')
colormap('jet');
c = colorbar;
c.Label.String = 'Isentropic Efficiency (%)';
grid on

%% Simulation function
function P_T_E = simu(P_H,m_flow,rpm)
   %% Defining Variables
   % Working Fluid's Operating Properties
   P_L = 1e5; % [Pa] proposed outlet pressure
   T_H = 350; % [K] proposed inlet temperature
   T_L = 298; % [K] proposed outlet temperature
   cp = 1.006e3; % [J/kg-K] for air
   cv = 0.73e3; % [J/kg-K] for air
   Rs = cp-cv;
```

```
% RVE Geometric Dimensions and Simulation Port Locations
R = 0.1; % [m] radius of large cylinder
e = 0.2*R; % [m] eccentric distance
z = 0.1; % [m] depth/length of rotor
Vanes = 4; %number of vanes
% Note: CCW is positive, so inport on the right and outport is on the left
in_port = deg2rad(wrapTo360(315:330)); % [rad] inlet port angle range
out_port = deg2rad(140:225); % [rad] outlet port angle range
n_rev = 4; % total number of revoultions
omega = rpm*(2*pi/60); % [rads/s]
sim =[0,2*pi*n_rev]; % simulation space


%% Establishing Control Volume
% Forming geometry
d_theta = 0:deg2rad(1):2*pi; % going CCW

% initialization
RR = zeros(1,length(d_theta));
for ii = 1:length(d_theta)
    RR(ii) = cal_L(e,R,d_theta(ii));
end

% Checking the radius of the rotor (rr)
rr(1,1:length(d_theta)) = mean([cal_L(e,R,3*pi/2),cal_L(e,R,pi/2)])-e;

% Integration in polar coordinate
% Defining function for upper bound of radial integration
upperBound = @(theta) sqrt(e^2+R^2-(2*e*R*cos(pi/2+theta-asin(cos(theta)*e/R))));
% Looping to find CV at theta of every 1/2 degrees
d_angle = deg2rad(0.5); % [rad] loop step angle
angles = sim(1):d_angle:sim(2); % [rad] range of stepped angles
d_vane = 2*pi/Vanes; % [rad] angle between vanes
V = zeros(1,length(angles));
% Performing integration for each angle and its storing volume
for ii = 1:length(angles)
    CV_ang = [angles(ii), angles(ii)+d_vane]; % integration bounds
    V(ii) = abs(integral2(@(theta, r) r, CV_ang(1),CV_ang(2), rr(1), upperBound)) *z;
end

%% Fitting Volume to a sine function for ODE
V_time = angles/omega;
[~, locs] = findpeaks(V,V_time);
amp = (max(V)-min(V))/2;
freq = 2*pi/mean(diff(locs));
shift = min(V)+amp;
phase = omega*wrapTo2Pi(locs(end))-(pi/2);

% Storing coefficients for use in derivative
trig_C = [amp;freq;phase;shift];
```

```
%% ODE45 Modelling
% ode conditions
max_step = 1.5e-4;
tspan = [V_time(1), V_time(end)-(2*pi/omega)];
options = odeset('MaxStep', max_step);

% setting time for each chamber (CV_t)
t_vane = d_vane/omega;
CV_t(1:Vanes,1) = linspace(V_time(1),V_time(1)+t_vane*(Vanes-1),Vanes);

% defining initial  conditions
V_int = amp*sin(freq.*CV_t-phase)+shift; % Inital Volume
T_int(1:Vanes,1) = T_L; % Inital Temp.
M_int = (P_L./(Rs.*T_int)).*V_int; % Inital Mass
L_int = zeros(4,1); % Inital Leakage
initial_C = [M_int;T_int;V_int;L_int]; % All intial conditions

% Other Constants for ODE
Port_C = [P_H, P_L,T_H, T_L];
R_interp = [d_theta;RR;rr]';

% Calling the ode45 function
% Note: M_T stores all thermodynamic properties and outputs of ode45
% Order is Mass,Temp,Volume, and Total Leakage; For all CVs
[t, M_T] = ode45(@(t,M_T)
odefun(t,M_T,d_vane,m_flow,Rs,cp,cv,Port_C,trig_C,R_interp,omega,Vanes,in_port,out_port),...
    tspan,initial_C,options);


%% Compiling results
theta = zeros(length(t),Vanes);
V_m = zeros(length(t),Vanes);
P_ms = zeros(length(t),Vanes);
for mm = 1:Vanes
    % Using time value from ode for all calculations and position estimate
    theta(:,mm) = t*omega+(mm-1)*d_vane;
    % Getting all Volume changes for specifc CV
    V_m(:,mm) = M_T(:,Vanes*2+mm);
    % Using Ideal gas law to solve for Pressure at every moment in time
    P_ms(:,mm) = (M_T(:,mm).*M_T(:,Vanes+mm)*Rs)./V_m(:,mm);
end
%% Torque calculations
% Calculating tangential distance for each vane. i.e. moment arm of pressure force
tan_r = (cal_L(e,R,theta)+rr(1))/2;
% Calculating the total area the pressure can act on each vane
tan_area = (cal_L(e,R,theta)-rr(1))*z;

torque = zeros(length(t),Vanes);
net_torque = zeros(1,length(t));
```

```
for ii = 1:length(theta(:,1))
    % Note: CCW is positive
    % Need to determine what pressures are acting on each vane
    for jj = 1:Vanes
        % defining the Pressure from Adjacent CV
        if jj == 1
            adj = Vanes;
        else
            adj = jj-1;
        end
        % individual torque calculations
        torque(ii,jj) = (P_ms(ii,adj)-P_ms(ii,jj)).*tan_area(ii,jj).*tan_r(ii,jj);
    end
    net_torque(ii) = sum(torque(ii,:)); % Total net torque at each moment in time
end

%% Friction modeling
% Centrifugal and spring forces only

% Defining constants for individual vane
spring_k = 5000; %[N/m] about 30lb/in
spring_l = 0.0675; %[m] spring free height
min_l = 0.025; %[m] length at max. compression
vane_l = rr(1)-min_l; %[m] length of the vane
vane_w = rr(1)*1/8; %[m] width of vane approximated
coef_f = 0.2; % coefficient of friction
rho_vane = 8000; %[kg/m^3] density if ss316 to find mass of
mass_vane = rho_vane*z*vane_l*vane_w;

% Alert user if spring is not long enough to maintain a force on it during maximum extension
if vane_l+spring_l < max(RR)
    error('Spring is not long enough to maintain vane contact with stator')
end

% Calculating friction values at each individual vane
compression_l = (vane_l+spring_l) - cal_L(e,R,theta); %[m] length the spring is compressed
f_spring = compression_l * spring_k; %[N] Spring force
% Centrifugal force below
f_centr = mass_vane.*(omega.*(cal_L(e,R,theta)-vane_l/2)).^2./(cal_L(e,R,theta)-vane_l/2); %[N]
f_fric =  (f_spring+f_centr)* coef_f; %[N] Frictional force
t_fric = f_fric.*cal_L(e,R,theta); %[N-m] Frictional torque lost
p_fric = f_fric.*omega.*cal_L(e,R,theta); %[W] Frictional power lost

% Net values of friction at every point in cycle
netT_fric = sum(t_fric,2); %[N-m]
netP_fric = sum(p_fric,2); %[W]
```

```
 % Final output values for function/specific interation
    power_output = mean(net_torque)*omega-mean(netP_fric);
    torque_output = mean(net_torque)-mean(netT_fric);
    meanT_H = mean(max(M_T(:,Vanes+1: Vanes*2)));
    meanT_L = mean(min(M_T(:,Vanes+1: Vanes*2)));
    isen_eff = (power_output/(m_flow*cp*(meanT_H-meanT_L)))*100;
    P_T_E = [power_output,torque_output,isen_eff ];
    %toc
end

%% ODE Function
function y =
odefun(t,M_T,d_vane,m_flow,Rs,cp,cv,Port_C,Trig_C,R_interp,omega,Vanes,in_port,out_port)
% defining position based on time
theta = t*omega;
% setting time and position for each chamber
CV_p(1:Vanes,1) = linspace(theta,theta+d_vane*(Vanes-1),Vanes);%Control V. position
CV_t = CV_p/omega; %Control V. position

% estimate for dV/dt
amp = Trig_C(1); freq = Trig_C(2); phase = Trig_C(3);
dVdt = amp*freq*cos(freq.*CV_t-phase);

% setting up location checks
Loc = zeros(Vanes,90);
for ll = 1:Vanes-1
    Loc(ll,:) = wrapTo2Pi(CV_p(ll):deg2rad(1):CV_p(ll+1)-deg2rad(1));
end
Loc(Vanes,:) = wrapTo2Pi(CV_p(end):deg2rad(1):CV_p(end)+d_vane-deg2rad(1));
Loc = round(rad2deg(Loc));

% Pressure calculations
P_H = Port_C(1); P_L = Port_C(2); T_H = Port_C(3); T_L = Port_C(4);
% Using Ideal gas: P = m*R*T/V
P_ms = (M_T(1:Vanes).*Rs.*M_T(Vanes+1:Vanes*2))./M_T(Vanes*2+1:Vanes*3);

%Leakage calculation
% Radius for leakage integration
RR = interp1(R_interp(:,1),R_interp(:,2),wrapTo2Pi(CV_p),'spline');
mu = 25e-6; %dynamic viscosity approx. for air at 450K, P not relevant
vane_w = R_interp(1,3)*1/8; %[m] width of vane approximated
rho_a = 0.785; % average density estimate
dP_dx = [P_ms(end)-P_ms(1);-diff(P_ms)]/vane_w; %P1-P2 for pressure drop, so -diff needed
gap = 0.1e-3; %[m]  estimated gap on both sides
% BCs and Integration Constant: u(y=0) = 0 and u(y=gap) = U = omega*r
% c2 = 0
% c1 = (U - (gap^2*dP_dx/(2*mu)))/gap;
```

```
% initialization
dmdt = zeros(Vanes,1);
dTdt = zeros(Vanes,1);
m_leak = zeros(Vanes,2);
for mm = 1:Vanes
    % Leakage integration needed in for loop
    % NSvelocity1 is for the 1st vane boundary of CV
    m_leak(mm,1) = (rho_a*gap*(RR(mm)-R_interp(mm,3))*(3*mu*omega*(RR(mm)+R_interp(mm,3))
...
        - dP_dx(mm)*gap^2))/(12*mu);

    % NSvelocity2 is for the front/next vane boundary of CV
    nn = mm + 1;
    if nn == Vanes +1
        nn = 1;
    end
    m_leak(mm,2) = (rho_a*gap*(RR(nn)-R_interp(nn,3))*(3*mu*omega*(RR(nn)+R_interp(nn,3)) ...
        - dP_dx(nn)*gap^2))/(12*mu);

    % determining what CV leaks in which direction for flow1
    if m_leak(mm,1) > 0 && mm > 1
        leak1 = mm -1;
    elseif m_leak(mm,1) > 0 && mm == 1
        leak1 = Vanes;
    elseif m_leak(mm,1) < 0
        leak1 = mm;
    else
        leak1 = NaN;
    end

    % determining what CV leaks in which direction for flow2
    if m_leak(mm,2) > 0
        leak2 = mm;
    elseif m_leak(mm,2) < 0 && mm == Vanes
        leak2 = 1;
    elseif m_leak(mm,2) < 0 && mm < Vanes
        leak2 = mm+1;
    else
        leak2 = NaN;
    end
```

```
   % Thermodynamics Calculations
   if any(ismember(Loc(mm,:),rad2deg(in_port))',1) %open inlet port
       inflow = m_flow*(P_H - P_ms(mm))/P_ms(mm);
       dmdt(mm,1) = inflow + m_leak(mm,1) - m_leak(mm,2);
       dTdt(mm,1) = (-P_ms(mm)*dVdt(mm) + cp*inflow*T_H + cp*m_leak(mm,1)*M_T(Vanes+leak1)
...
           - cp*m_leak(mm,2)*M_T(Vanes+leak2)-
cv*dmdt(mm)*M_T(Vanes+mm))*(1./(M_T(mm)*cv));
   elseif any(ismember(Loc(mm,:),rad2deg(out_port))',1) % open outlet port
      outflow = m_flow*(P_L - P_ms(mm))/P_ms(mm);
       dmdt(mm,1) = outflow + m_leak(mm,1) - m_leak(mm,2);
       dTdt(mm,1) = (-P_ms(mm)*dVdt(mm) + cp*outflow*M_T(Vanes+mm) +
cp*m_leak(mm,1)*M_T(Vanes+leak1) ...
           - cp*m_leak(mm,2)*M_T(Vanes+leak2)-
cv*dmdt(mm)*M_T(Vanes+mm))*(1./(M_T(mm)*cv));
   else %ports closed, only leakage
       dmdt(mm,1) = (m_leak(mm,1)-m_leak(mm,2));
       dTdt(mm,1) = (-P_ms(mm)*dVdt(mm)+ cp*m_leak(mm,1)*M_T(Vanes+leak1) ...
           - cp*m_leak(mm,2)*M_T(Vanes+leak2)-
cv*dmdt(mm)*M_T(Vanes+mm))*(1./(M_T(mm)*cv));
   end
end

y = [dmdt;dTdt;dVdt;m_leak(:,1)-m_leak(:,2)];

end

%% Dimensioning function
function L = cal_L(e,R,theta)
L = sqrt(e^2+R^2-(2*e*R.*cos(pi/2+theta-asin(cos(theta).*e/R))));
end
```

BIBLIOGRAPHY

[1] Z. Gnutek and P. Kolasinski, "The Application of Rotary Vane Expanders in Organic Rankine Cycle Systems-Thermodynamic Description and Experimental Results," *JOURNAL OF ENGINEERING FOR GAS TURBINES AND POWER-TRANSACTIONS OF THE ASME,* vol. 135, no. 6, pp. 1-10, 2013.

[2] P. Kolasinski, P. Blasiak, and J. Rak, "Experimental and Numerical Analyses on the Rotary Vane Expander Operating Conditions in a Micro Organic Rankine Cycle System," (in English), *Energies,* vol. 9, no. 8, p. 606, 2016 2016.

[3] C. Xia, W. Zhang, G. Bu, Z. Wang, and P. Shu, "Experimental study on a sliding vane expander in the HFC410A refrigeration system for energy recovery," *Applied Thermal Engineering,* vol. 59, no. 1, pp. 559-567, 2013/09/25/ 2013.

[4] J. Xiaohan, Z. Bo, Y. Bingchun, and P. Xueyuan, "Study of a Rotary Vane Expander for the Transcritical CO2 Cycle-Part II: Theoretical Modeling," *HVAC&R Research,* Article vol. 15, no. 4, pp. 689-709, 2009.

[5] C. National Research, "Solar System Exploration Today: A Multifaceted Endeavor," in *New Frontiers in the Solar System: An Integrated Exploration Strategy*Washington, DC: National Academies Press, 2003, pp. 153-174.

[6] A. T. Basilevsky and J. W. Head, "The surface of Venus," *Reports on Progress in Physics,* vol. 66, no. 10, pp. 1699-1734, 2003.

[7] D. M. Hunten, "Venus: Atmosphere," in *Encyclopedia of the Solar System*, L.-A. McFadden, P. R. Weissman, and T. V. Johnson, Eds. 2nd ed. ed. Amsterdam: Elsevier, 2007, pp. 139-148.

[8] E. Kolawa, *Extreme environment technologies for future space science missions*. National Aeronautics and Space Administration, Jet Propulsion Laboratory, California Institute of Technology, 2007.

[9] C. National Research, "Inner Solar System: Key to Habitable Worlds," in *New Frontiers in the Solar System: An Integrated Exploration Strategy*Washington, DC: National Academies Press, 2003, pp. 39-66.

[10] J. N. Hodgson, *Experimental investigation of the SNAP-8 mercury Rankine-cycle power conversion system* (no. Book, Whole). 1969.

[11] G. Bianchi and R. Cipollone, "Friction power modeling and measurements in sliding vane rotary compressors," *Applied Thermal Engineering,* vol. 84, pp. 276-285, 2015.

[12] G. Bianchi and R. Cipollone, "Theoretical modeling and experimental investigations for the improvement of the mechanical efficiency in sliding vane rotary compressors," *APPLIED ENERGY,* vol. 142, pp. 95-107, 2015.

[13] P. Kolasinski, "The Influence of the Heat Source Temperature on the Multivane Expander Output Power in an Organic Rankine Cycle (ORC) System," *ENERGIES,* vol. 8, no. 5, pp. 3351-3369, 2015.

[14] B. Yang, X. Peng, Z. He, B. Guo, and Z. Xing, "Experimental investigation on the internal working process of a CO2 rotary vane expander," *Applied Thermal Engineering,* vol. 29, no. 11, pp. 2289-2296, 2009/08/01/ 2009.

[15] J. Walker, R. Resnick, and D. Halliday, *Fundamentals of physics*, Tenth, extend ed. (no. Book, Whole). Hoboken, NJ: John Wiley & Sons, Inc, 2014.

[16] "MATLAB," 2017B ed. Natick, Massachusetts, United States: The MathWorks, 2018.

ACADEMIC VITA
BRYANT WARMATE

btwarmate@outlook.com

Education:

Bachelor of Science in Mechanical Engineering Spring 2018
The Pennsylvania State University
Schreyer Honors College

Thesis Title: Numerical Modelling of a Rotary Vane Expander for a Power Cycle on a Proposed Landed Mission to Venus
Thesis Supervisor: Dr. Alex Rattner

Engineering Experience:

United Technologies (Otis), CT *Suspension & Systems Intern* (May – Aug. 2017)

- Designed, tested and computed the damping properties of various CSBs (Suspension Belts)
- Collaborated to apply root-cause analysis that improved dynamic system modelling accuracy by 40%
- Optimized test procedure to improve efficiency and safety, resulting in a 20% decrease in worktime

Enviro-Tech Systems, LA *Shop & Office Intern* (June – Aug. 2015)

- Actively engaged in the machine shop and gained hands-on experience of the production process
- Assisted a Petroleum Engineer in planning and sizing 5 successful oil separation units for oil platforms
- Proactively minimized downtime by maintaining an inventory of all parts, and restocked parts as needed

Research Experience:

Schreyer Honor Thesis, Dr. Rattner *Modelling of a Rotary Vane* (Dec 2016 – to date)

- Formulated a detailed thermodynamic analysis of the Rotary Vane Expander for multiple working fluids
- Modelled theoretical performance of Rotary Vane using medium order differential equations in MATLAB

Undergraduate Research, Dr. Gamberg *Nuclear Particle Theory* (August 2015 – Dec 2016)

- Utilizing Python to perform data analysis on experimental data of subatomic particles. Presented the progress and results in the Vancouver (Canada) 2016 APS Division of Nuclear Physics conference

Multi-Campus REU, Dr. Panah *Boundary Layer Flow* (May – Aug. 2016)

- Designed dynamic mechanisms to study fluid flow over oscillating surfaces such as a flapping wing
- Presented final iteration in the Research Experience for Undergraduates (REU) conference

Leadership Positions:

Program Assistant & Tutor *Engr. Ahead Program (NSF Grant)* (June 2016 & 2018)

- Led a jump-start program for 20 incoming minority engineering students to a success rate of 80%

Director of Membership *Berks Blue & White Society* (April 2015 – May 2016)

- Planned events with alumni to increase networking with students and increased membership by 75%

Technical Skills & Software:

- SolidWorks/CAD Modelling
- Basic 2D P&ID Drafting
- MATLAB
- Microsoft Excel

Honors & Involvement:

- Tau Beta Pi Engineering Honors Society (Jan. 2018 – to date)
- National Society of Black Engineers (NSBE) – Outreach division/Step-Up (Jan. 2017 – to date)
- Dean's List: Every Semester (Apr. 2015 – 2018)
- Penn State Scholastic Award: Freshman, Junior & Senior Years (Apr. 2015, 2017 & 2018)
- Change of Campus Leadership Conference – Program Assistant & Mentor (Aug. 2017)
- United Way: Collaboratively sought donors for UTC silent auction (July 2017)
- Penn State Berks Math, Physics & 1st Year Chemistry Award (May 2015 & 2016)
- Valedictorian: Great Lakes Christian High School (June 2014)